

ABSTRACT

LU, XINYUE. Multiple Layer Nerve Guide for Peripheral Nerve Regeneration Using Carbon Nanotubes. (Under the direction of Martin W. King).

When a motor, sensory or sympathetic peripheral nerve has been damaged, injured or severed, there are currently a number of therapies to reconnect the proximal end to the distal stump. Some of these treatments involve the use of a resorbable tubular nerve guide that not only serves as a conduit to enable the proximal neurons to grow in the direction of and eventually reconnect to their distal partner, but also protects the axons and Schwann cells from being diverted from their desired pathway by the inflammatory response of infiltrating macrophages and fibroblasts. Nerve guide conduits have the potential to be the preferred option in clinical nerve repair for gaps of up to 30 mm. The key to successful treatment for a peripheral nerve lesion is to lead the axonal regeneration towards the distal endoneural stump, where after reconnection electrical signals can reestablish the neural function. In addition, the nerve guide must have sufficient compression resistance to serve as a protective envelope around the nerve during the period of nerve regeneration. Polylactic acid (PLA) braided tubes are flexible, biocompatible and biodegradable. Carbon nanotubes (CNTs) are nano-scale materials with electrical conductivity. In this study, by including aligned carbon nanotubes within a double layer PLA braided structure, we concluded that the presence of the carbon nanotubes improved the tensile strength, compression resistance and kink recovery of the prototype nerve guides. In order to evaluate the biological performance, the nerve guide samples were cultured in vitro for 7 days with 3T3 fibroblast cells. All four nerve guide prototypes were found to be biocompatible and provide equivalent conditions for

the proliferation and attachment of fibroblasts regardless of whether they included carbon nanotubes or not. However, the cells did not migrate along the alignment direction of the CNTs. This may require an externally applied electrical potential. Even so, this multiple layer nerve guide using aligned carbon nanotubes has the potential to be used for peripheral nerve regeneration.

© Copyright 2014 by Xinyue Lu

All Rights Reserved

Multiple Layer Nerve Guide for Peripheral Nerve Regeneration
Using Carbon Nanotubes

by
Xinyue Lu

A thesis submitted to the Graduate Faculty of
North Carolina State University
in partial fulfillment of the
requirements for the degree of
Master of Science

Textile Engineering

Raleigh, North Carolina

2014

APPROVED BY:

Dr. Martin W. King
Committee Chair

Dr. Zhen Gu

Dr. Wendy E. Krause

Dr. Natasha Olby

DEDICATION

To my parents, friends and members of the BMT group!

BIOGRAPHY

Xinyue Lu received her B.E. in Textile Engineering in July 2012 from Donghua University, Shanghai, P. R. China. She came to North Carolina State University for graduate program in Textile Engineering in August 2012. She was elected to be the public relation officer for the Textile Association for Graduate Students from May 2013 to May 2014. And she is expected to receive her Master of Science degree in August 2014. She has a great passion for biomedical devices, especially biomedical textiles. She is going to continue her study for a PhD degree in the area of bioengineering, especially in biomaterials. Her career goal is to be a faculty member in a university and do research in the area of biomaterials.

ACKNOWLEDGMENTS

I would like to express my thanks to all the people who helped with my research. First of all, I sincerely thank Dr. Martin W. King for his constant support, funding, guidance and encouragement not only in my study in NC State, but also in my future career. His dedication and enthusiasm for his work inspire all his students. His love and care for us affects every member in our research group.

I would also like to give my appreciation to my other committee members, Dr. Wendy E. Krause, Dr. Natasha Olby and Dr. Zhen Gu for their encouragement and guidance. Many thanks to Dr. Zhen Gu for his generosity in letting me use his laboratory supplies. In addition, I would like to give special thanks to Dr. Philip Bradford in the College of Textiles for his generosity in providing carbon nanotubes. Many thanks to Ozkan Yildiz, a graduate student of Dr. Bradford for fabricating the special aligned carbon nanotubes in electrospun poly(ethylene oxide) webs.

I also would like to express my thanks to all the members of Dr. Martin King's Biomedical Textiles Group and all the technicians and researchers who have helped me with my study: William Barnes, Valerie Knowlton and Dr. Eva Johannes. I must also express my appreciation to my friends for their love and encouragement, especially those who after prepared meals for me when I was busy. Last but not the least, I must give thanks to my parents for supporting me to study in the US.

TABLE OF CONTENTS

LIST OF TABLES	vii
LIST OF FIGURES.....	viii
CHAPTER 1	1
GENERAL INTRODUCTION	1
1.1 Background and Motivation	1
1.2 Objectives and Hypotheses	3
1.3 Significance	6
CHAPTER 2	8
REVIEW OF LITERATURE.....	8
2.1 Nervous System.....	8
2.2 Injuries to the Peripheral Nervous System.....	11
2.3 Categories of Peripheral Nerve Regeneration	15
2.3.1 Direct Repair	16
2.3.2 Autografting	17
2.3.3 Neural Scaffolds.....	18
2.3.4 Allografts	19
2.4 Biomaterials for Nerve Regeneration	19
2.4.1 Polylactic acid (PLA).....	20
2.4.2 Polyglycolic Acid (PGA).....	22
2.4.3 Polylactic-co-glycolic Acid (PLGA).....	23
2.4.4 Poly (ϵ -caprolactone) (PCL).....	24
2.4.5 Type I Collagen.....	25
2.5 Carbon Nanotubes (CNTs) for Nerve Regeneration.....	27
2.5.1 Properties of Carbon Nanotubes (CNTs).....	27
2.5.2 Synthesis of CNTs.....	30
2.5.3 Toxicity of CNTs	32
2.5.4 CNTs for Nerve Regeneration.....	32
CHAPTER 3	35
MATERIALS AND METHODS	35
3.1 Fabrication of Nerve Guides	35
3.1.1 Preparation of Electrospun Poly(ethylene oxide) and CNTs	36
3.1.2 Braiding Nerve Guides.....	37
3.1.3 Post Processing.....	40
3.1.4 Total porosity and pore size	42
3.2 Evaluation of Physical Properties of Nerve Guides	44

3.2.1 Tensile Strength and Elongation at Break.....	44
3.2.2 Kink Resistance and Recovery	45
3.2.3 Compression Resistance and Elastic Recovery	46
3.2.4 Suture Retention Strength.....	48
3.3 Biological Performances of Nerve Guides	50
3.3.1 Sample Preparation	50
3.3.2 Preparation and Harvesting 3T3 Fibroblast Cells	51
3.3.3 Seeding 3T3 Fibroblast Cells on the Nerve Guides.....	52
3.3.4 Cell Proliferation by MTT Assay.....	52
3.3.5 Live/Dead Proliferation and Migration of Cells by Laser Scanning Confocal Microscope	54
3.3.6 Cells Attachment by Scanning Electron Microscope	55
3.4 Statistical and Analysis	57
CHAPTER 4.....	58
RESULTS AND DISCUSSION	58
4.1 Basic Properties of Multiple Layer Nerve Guides.....	58
4.1.1 Structure of Multiple Layer Nerve Guides.....	58
4.1.2 Braiding Parameters for the Braided Nerve Guides.....	60
4.2 Physical Properties	62
4.2.1 Porosity and Pore Size.....	62
4.2.2 Tensile Strength and Elongation at Break.....	64
4.2.3 Kink Resistance and Recovery	68
4.2.4 Compression Resistance and Recovery	70
4.2.5 Suture Retention.....	74
4.3 Biological Performance	76
4.3.1 Cell Viability and Proliferation by MTT Assay for Biocompatibility	76
4.3.2 Cell Migration and Proliferation of Live/Dead by LSCM.....	78
4.3.3 Cell Attachment of SEM	84
CHAPTER 5.....	87
CONCLUSIONS AND FUTURE WORK.....	87
5.1 Conclusions	87
5.2 Future Work.....	89
REFERENCES.....	91

LIST OF TABLES

Table 2.1 Classification of the six degrees of nerve injuries	13
Table 4.1 Braided structure for each nerve guide prototype	62
Table 4.2 Total of porosity and average pore size for four nerve guide prototypes	63
Table 4.3 Results of tensile strength	65
Table 4.4 Results of radial compression and recovery testing	71
Table 4.5 Results of suture retention strength.....	75
Table 4.6 Absorbance results from MTT assay	76

LIST OF FIGURES

Figure 2.1 Neuron structure.....	9
Figure 2.2 Schwann cells.....	10
Figure 2.3 Structure inside the entire nerve trunk.....	11
Figure 2.4 Formation of bands of Bünger.....	14
Figure 2.5 Various treatments for nerve repair.....	16
Figure 2.6 Commercial nerve guide conduits.....	20
Figure 2.7 (a-b) Synthesis, chemical structure of PLA.....	21
Figure 2.7 (c) Stereoforms of lactic acid.....	21
Figure 2.7 (d) Stereoforms of lactide by ring-opening polymerization.....	21
Figure 2.8 Chemical structure of PGA.....	23
Figure 2.9 Chemical structure of PLGA.....	24
Figure 2.10 Chemical synthesis of PCL.....	25
Figure 2.11 (a-b) Structure of fullerene and graphene.....	27
Figure 2.12 (a) Structures of SWNTs determined by the indices n and m.....	29
Figure 2.12 (b) Structure of MWNTs.....	29
Figure 3.1 Flow chart of fabrication process.....	35
Figure 3.2 Structure of electrospun PEO/CNTs.....	37
Figure 3.3 (a-b) Central core and braiding machine.....	38
Figure 3.4 (a-b) Second central core and second braiding process.....	40
Figure 3.5 (a) View of specimens after pulling out black PP monofilament sutures.....	41

Figure 3.5 (b) Braided structure of final nerve guides.....	41
Figure 3.6 Cross section observed by microscope (4×).....	43
Figure 3.7 (a-b) Tensile testing	45
Figure 3.8 Kink resistance testing.....	46
Figure 3.9 Compression resistance test	47
Figure 3.10 (a-c) Suture retention testing	49
Figure 3.11 Nerve conduits at the length of 10 mm.....	50
Figure 3.12 (a-c) Equipment for preparation and operation of scanning electron microscope	56
Figure 4.1 (a-c) Images showing structure of 200 CNT sample.	59
Figure 4.1 (d-e) Cross-sectional images showing structure of 200 CNT sample and PEO sample.	60
Figure 4.2 (a) Tensile strength results: maximum load.....	65
Figure 4.2 (b) Percent elongation at break.....	66
Figure 4.3 Comparison of load/elongation curves	67
Figure 4.4 Kink resistance test	69
Figure 4.5 (a-b) Prototype nerve guide samples before and after kink resistance testing.	70
Figure 4.6 (a) Compression resistance test results	72
Figure 4.6 (b) Compression recovery test results.....	72

Figure 4.7 Comparison of the levels of compression resistance and compression recovery.....	73
Figure 4.8 Comparison of suture retention strength.....	75
Figure 4.9 Results of MTT assay on Day 1, Day 3 and Day 7.....	77
Figure 4.10 (a) Four images for the CONTROL sample on Day 7:.....	79
Figure 4.10 (b) Combined image of the CONTROL sample showing the live and dead cells without the PLA layer after Adobe Photoshop correction.....	80
Figure 4.11 (a-d) Live and dead cells on the inner PLA layer for the four different nerve guide samples on Day 7.....	81
Figure 4.12 (a-b) Images represent 3T3 cell viability on the CNTs on Day 7.....	83
Figure 4.13 (a) Cells attached to the CNT web of the 100 CNT sample.....	84
Figure 4.13 (b) Cells attached to the CNT web of the 100 CNT sample.....	84
Figure 4.13 (c) Cells attached to the CNT web of the 200 CNT sample.....	85
Figure 4.13 (d) Single cell attachment to the CNT web on the 200 CNT sample.....	85
Figure 4.13 (e) Single cell attachment to the CNT web of the 200 CNT sample.....	85
Figure 4.14 (a) 3T3 cells on the inner PLA tube. Scale bar: 100µm.....	86
Figure 4.14 (b) A single 3T3 cell attached and aligned on the PLA fibers.....	86

CHAPTER 1

GENERAL INTRODUCTION

1.1 Background and Motivation

The incidence of peripheral nerve injury is currently a critical health issue. Such injuries can be caused by contusion, stretching, laceration or burns. They cover approximately 2.8% of trauma cases and result in almost \$150 billion in annual healthcare costs in the United States alone (Santin, 2009). The type and extent of the nerve injury determines the way and degree to which the nerve will recover. If the lesion involves axonal injury as well as surrounding connective tissue damage, spontaneous regeneration of the damaged nerve may not happen (Zochodne, 2008). In this case, surgical peripheral nerve repair is required. Currently autografting is regarded as “the gold standard” for neural restoration. However, morbidity at the donor site is a crucial issue. To solve this problem, artificial nerve guides have the potential to be an attractive option in peripheral nerve repair (Griffin, Hogan, Chhabra, & Deal, 2013).

There are three main advantages of artificial nerve guides for peripheral nerve repair. First, it overcomes the lack of available autografts and avoids morbidity at the donor site. Second, the nerve guide can serve as a conduit to enable the axons and Schwann cells to grow in the right direction and so eventually reconnect to their distal partner. Third, it protects the axons and Schwann cells from being diverted from the desired pathway by the inflammatory response of infiltrating macrophages. As such it provides a protective envelope around the nerve during the period of nerve regeneration as it migrates and reconnects with its distal stump. Eleven commercial nerve guide devices, including nerve guide conduits and nerve protective wraps have been approved by the FDA since 1995 (Kehoe, Zhang, & Boyd, 2012). However, some commercial nerve guide conduits are too rigid, such as the Neurolac[®] device, or the rate of degradation is too fast, such as the Neurotube[®], resulting in a loss of stable architecture during the regeneration process. These devices have been associated with a chronic inflammatory response and nerve guide compression. Therefore, a flexible and semi-permeable nerve guide with improved compression resistance and an acceptable degradation rate is important for nerve guide design.

Since neurons are electrically stimulated, the conductivity may improve the extent of neuronal growth by introducing a conductive material into the flexible and semi-permeable artificial nerve (Huang, Wu, Tai, & Wang, 2012). In addition, conductivity has

the potential to enhance the rate of nerve regeneration. Carbon nanotubes are nanomaterials that have been widely applied in the field of neuroscience research for repairing both central nerves and peripheral nerves in recent years. Carbon nanotubes and their composites have already been shown to increase neuronal adhesion and promote cell differentiation as well as result in a low immunogenic profile (Fabbro A, Sucapane A, & etc, 2013). Therefore, we are proposing to fabricate a flexible nerve guide that has good compression resistance and contains carbon nanotubes to improve the rate and the extent of nerve regeneration. The flexible structure can be achieved by using a braiding technique to create a double layer hollow tube with a higher outer layer density so that the compression resistance can be enhanced (J. Liang, 2013).

1.2 Objectives and Hypotheses

The ultimate goal of this study is to fabricate and evaluate the physical properties and nerve regeneration performance of multiple layer nerve guides made from polylactic acid (PLA) and incorporating aligned carbon nanotubes. However, before reaching this ultimate goal, the first objective is to evaluate the biocompatibility of this special multiple layer structure with aligned carbon nanotubes. Therefore, the main aim for this research is to fabricate the multiple layer nerve guide conduit using directional carbon nanotubes and evaluate its mechanical and biocompatible behavior. In order to align the carbon

nanotubes in one direction, they need to be co-electrospun into an orientated web with a second material, which in this case, will be poly(ethylene oxide) polymer.

Three specific objectives have been proposed as listed below, followed by a description of the tests that will be needed for their evaluation.

1. To design and fabricate multiple layer nerve guide prototype samples with and without directional carbon nanotubes using braiding technology.
 - a) To review the literature for the types of fabrication and the types of polymers and carbon nanotubes that have been used to prepare nerve guides.
 - b) To discuss the general requirements and appropriate resorbable polymers for nerve guide fabrication based on a review of the literature.
 - c) To select the yarns, design the structure, and set the braiding parameters for this experimental study and define the independent and dependent variables. Four prototype samples were designed and fabricated: i) nerve guide with 100 layers of carbon nanotube/poly(ethylene oxide) composite web, ii) nerve guide with 200 layers of carbon nanotube/poly(ethylene oxide) composite web, iii) nerve guide with no carbon nanotubes and only a poly(ethylene oxide) web and iv) an empty hollow control sample nerve guide with no web added.
2. To evaluate the mechanical properties of the four prototype samples and compare the performance of the nerve guides with and without carbon nanotubes.

- a) To perform mechanical tests and the four prototype samples, including a tensile strength test, compression resistance and compression recovery tests, a kink resistance test and a suture retention test.
 - b) To analyze any differences between the four prototype samples using statistical analysis.
3. To evaluate the biocompatibility of the nerve guide prototype samples with and without carbon nanotubes using 3T3 fibroblast cells.
- a) To perform a biological test by culturing 3T3 cells for 7 days on the four prototype samples of nerve guides and evaluate their cell proliferation by MTT assay, their cell viability and extent of migration by a live/dead assay using laser scanning confocal microscopy (LSCM), and their degree of cell attachment by scanning electron microscopy (SEM).
 - b) To compare the biological performance of the four prototype samples and analyze any differences between them using statistical analysis.

According to the objectives, I hypothesize that:

1. The braided structure will protect the carbon nanotube layer from structural changes during the process of heat setting so as to maintain their stability during the liquid culture environment.

2. The use of carbon nanotubes will improve the mechanical properties, such as tensile strength and compression resistance, and the higher concentration of carbon nanotubes in the nerve guide sample will yield superior results.
3. The process of introducing and removing the poly(ethylene oxide) webs will not affect the mechanical and biological properties of the nerve guides.
4. The nerve guide samples with carbon nanotubes are biocompatible.
5. The directional alignment of the carbon nanotubes will help the cells migrate along the axial direction of the nerve guides.

1.3 Significance

There are two significant points in this study. First, based on the prior study of a double layer flexible and semi-permeable nerve guide, it is proposed that the axially aligned carbon nanotubes will be protected from any external environmental damage. The structure works as a capsule to enclose the directional carbon nanotubes and holds them in position without altering the flexibility of the nerve guide. Second, the two layer braided structure presents a high surface area of pure directional carbon nanotubes to the neural cells and provides superior mechanical performance. Based on past studies focused in the literature, when nerve guides have incorporated pure carbon nanotubes, they have only been present in the form of a web or twisted yarn. In these cases, the two-

dimensional web could not represent the properties of a tubular structure of a nerve guide and the twisted yarn had inferior mechanical properties compared to the braided polymer tube (Huang, 2012).

CHAPTER 2

REVIEW OF LITERATURE

2.1 Nervous System

The nervous system is composed of the central nervous system (CNS) and the peripheral nervous system (PNS) and is formed from a network of neurons and neuroglia. Specialized types of neurons, called sensory neurons, collect information from the environment by responding to touch, sound, light and other stimuli that effect our sensory organs and send it to the central nervous system, which is the brain and spinal cord. Our brain and spinal cord, which are responsible for regulating our bodily functions, interpret this information and generate responses that are transmitted through motor neurons to cause muscle contraction, affect glandular output and stimulate the neural network (Carbrey, 2014).

Neurons are electrically excitable cells in the nervous system that receive and respond to the stimulus of electrical signals along their length as well as transfer information by chemical signals with other neurons. A typical neuron is formed from a cell body soma, dendrites and a single axon (Figure 2.1). Axons can pass information between neurons, but dendrites can only receive information from other neurons and send the information

to the cell body. There are junctions between each neuron (presynaptic neurons and postsynaptic neurons) to transmit signals, which are called synapses. For a single neuron, the synaptic input is received by the cell body or dendrite, but it is then transmitted from the axon to other neurons.

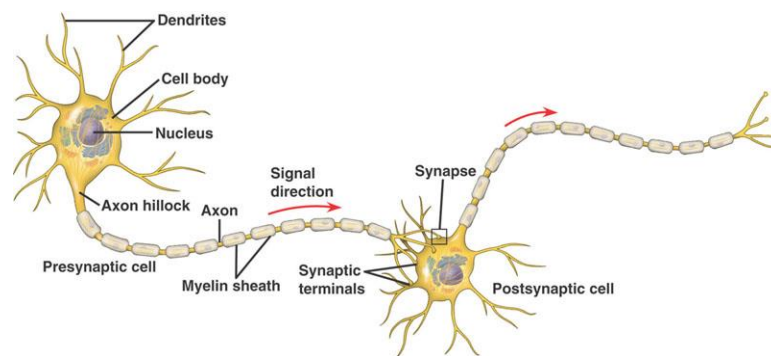


Figure 2.1 Neuron structure

(Copyright: Kennesaw State University)

There are several types of glial cells, sometimes called neuroglia, that do not transmit the stimuli but support the neurons in several different ways. First, they surround the neurons and maintain their position. They also provide nutrients and oxygen, and insulate neurons from each other. A dielectric plasma membrane, called myelin sheath, is formed by glial cells. It surrounds the axon of each neuron and provides insulation for the electrical signals. In the peripheral nervous system, Schwann cells, which are generated from the multipotent neural crest cells, cover the axons by wrapping them with myelin (Figure 2.2). They are critical for the regeneration of the peripheral nervous

system, and as a result, research in peripheral nerve regeneration mainly focuses on the proliferation of Schwann cells (Brenner, Lowe, & Fox, 2005).

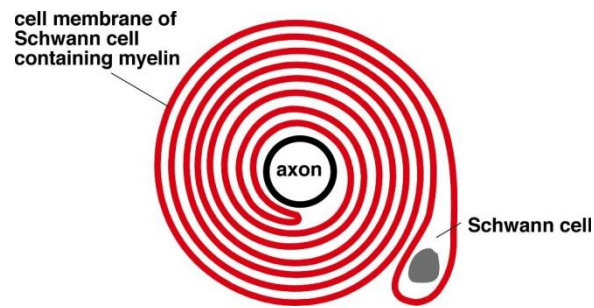


Figure 2.2 Schwann cells

(Copyright: Sciprojex)

In the peripheral nervous system, the Schwann cells that cover the axon with a myelin sheath form a nerve fiber. The nerve fibers, called fascicles, are organized in bundles. In a single nerve, there may be up to 3,400 fascicles (Birch, 2013). The rich and oriented endoneurial collagen in peripheral nerves makes them strong and resilient for surgeons to perform clinical interventions. And for this reason the addition of collagen coating makes the use of nerve conduit a more attractive therapy for nerve repair. Outside the fascicles, there are three protecting layers: the inner endoneurium, the perineurium and the outer epineurium. The axons support themselves inside the inner layer of endoneurium. The perineurium is located around each fascicle and holds the bundle of axons together to prevent them from separating. The epineurium is a connective tissue, composed of collagen fibers, mass cells and fibroblasts that envelops the entire nerve trunk (Figure 2.3).

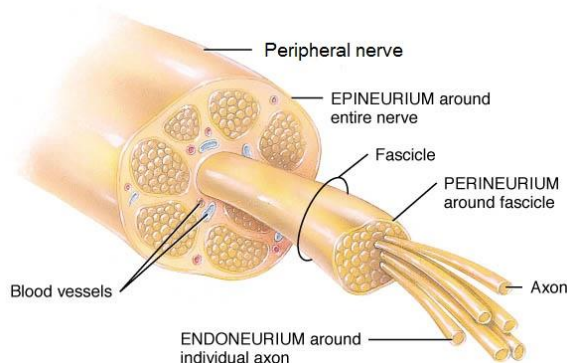


Figure 2.3 Structure inside the entire nerve trunk

(Copyright: Adapted (Schmid, 2012))

2.2 Injuries to the Peripheral Nervous System

The type of nerve injury determines the way in which spontaneous regeneration might occur. According to Sir Herbert Seddon, three types of nerve injuries were classified in 1943 as: neurapraxia (Class I), axonotomesis (Class II) and neurotomesis (Class III) (Evans, 2001). Neurapraxia is the least severe form of injury and usually leads to complete recovery. It is a lesion with no associated axonal injury but with an interruption in conduction, which means that Wallerian degeneration or local damage of axons from other causes does not occur. So it can be repaired completely after the cause has been removed. Axonotomesis is a degenerative lesion with some axonal injury, but without damage to connective tissues or the epineurium of the nerve. In this type of crush injury, the basal lamina of the Schwann cells is maintained and the proximal axon can regenerate

and reconnect to the distal Schwann cells if the correct path can be found. The third type of injury, called neurotmesis, is the most severe lesion. It is often the result of severe contusion, stretching, laceration or local anesthetic toxicity. In this case, the degenerative lesion not only involves axonal injury, but also there is damage to the surrounding connective tissue and epineurium, which has caused separation between the distal and proximal stumps (Zochodne, 2008). Wallerian degeneration has affected the cell body and the Schwann cells. Therefore, spontaneous regeneration is unlikely to occur at all.

In addition to the classification by Seddon, more recently Sunderland has expanded this three class system to include five degrees of nerve injury. A first-degree injury is the same as neurapraxia. It is without axon damage or Wallerian degeneration, and is associated with only local demyelination and a temporary block in axonal conduction (Zochodne, 2008). A second-degree injury is the same as axonotmesis and relates to damage of the axon with distal Wallerian degeneration, but without disruption to the basal lamina or endoneurium. A third-degree injury refers to the interruption of axonal continuity with endoneurial disruption, but the perineurial sheath remains intact. Natural recovery from this degree of injury is sometimes possible. A fourth-degree injury is the disruption of the nerve trunk but without separation of the epineurium, which remains intact. This means that the nerve trunk is still in a continuous form. A fifth-degree injury is the same as neurotmesis, with total separation of the nerve trunk. In addition, Dellon and MacKinnon have added a sixth-degree injury, which involves a combination of different types of

injury to individual fascicles, with local demyelination and axonal degeneration. Table 2.1 below shows the classification of the different levels of injury. Injuries of the first, second and third degree can recover by themselves. But fourth, fifth and sixth degree injuries, surgical treatment is required (Ray & Mackinnon, 2010)

Table 2.1 Classification of the six degrees of nerve injuries

Degree	I	II	III	IV	V	VI
Name of injury	Neurapraxia	Axonotmesis		Neurotmesis		
Axonal		x	x	x	x	x
Endoneurial			x	x	x	x
Perineurial				x	x	x
Epineurial					x	x
Wallerian Degeneration		x	x	x	x	x
Recovery	complete	complete	incomplete	none	none	none

Overall, from the clinical point of view, the key to successful treatment of peripheral nerve lesions is to guide axonal regeneration into the distal endoneurial tube. Following a nerve injury, the proximal and distal stumps experience changes in their structure and release bio-molecules that assist in axonal regeneration (Sulaiman & Gordon, 2013). The injured axon develops axonal sprouts, and these sprouts elongate towards the distal

nerve stumps. In the regions where the axon is still intact, myelinated and unmyelinated fibers sprout new axons with a basal lamina that form a regenerating unit (Santin, 2009). Initially there are cytoskeletal materials and transported cytoskeletal proteins which support the first stage of regeneration. Then the Schwann cells direct the regeneration of the axon along the endoneurial channel, which is referred to as the bands of Bünger. The image in Figure 2.4 shows the formation of bands of Bünger. The Schwann cells phagocytize the axonal and myelin debris and secrete chemoattractive factors to attract macrophages into the distal nerve stumps. Together they help phagocytize the axonal and myelin debris during the regeneration process. The axonal debris releases mitogens that stimulate the division of the Schwann cells. In this way the axonal sprouts, the axons and the Schwann cells establish a close relationship to facilitate the regeneration process.

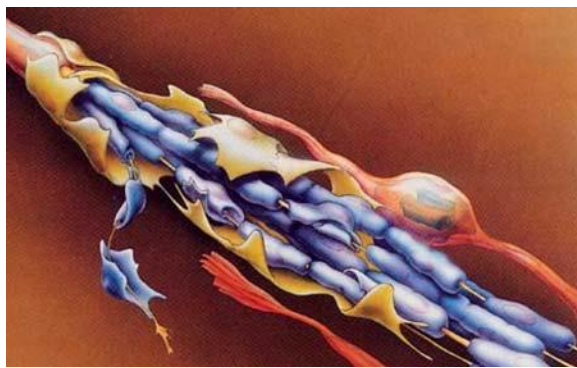


Figure 2.4 Formation of bands of Bünger.

Schwann cells: blue; Regenerating sprouts: yellow; Basal lamina: orange

(Copyright: (Mackinnon & Dellon, January, 1988))

2.3 Categories of Peripheral Nerve Regeneration

Peripheral nerve injury is a critical health issue for our society, which affects approximately 2.8% of trauma cases, resulting in nearly \$150 billion in annual health care cost in the United States alone (Santin, 2009). Around 100,000 patients in the United States and Europe need a neurosurgical intervention for a peripheral nerve injury each year. Successful functional recovery of peripheral nerve injuries is often incomplete and leads to a subsequent reduced quality of life. The proper clinical treatment can only be determined after a clinical evaluation of the type and level of injury (Figure 2.5). If direct tensionless end-to-end repair can reconnect the damaged nerve, it is considered the preferred surgical peripheral nerve repair. For the longer gaps where direct suturing may cause tension, autografting is the standard of care for neural restoration. However, nerve autografting usually leads to morbidity at the donor site and the lack of suitable donor tissue is also a limitation. To solve these problems of autografting, the development of an artificial conduit for the regeneration of the nerve between the proximal and distal stumps is an alternative approach to clinical treatment. Neural scaffolds have the potential to be an attractive option for the repair of nerve gaps up to 30 mm wide. For longer nerve regeneration, allografts have been shown experimentally to provide an alternative strategy (Griffin et al., 2013). Other therapies for repairing peripheral nerve injury include the use of fibrin glue and cell based therapies with growth factors (Li et al., 2014).

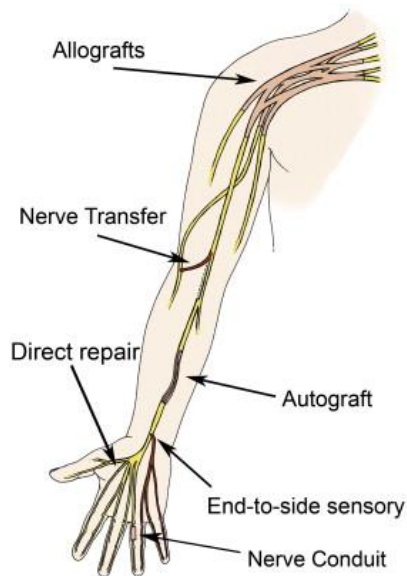


Figure 2.5 Various treatments for nerve repair

(Copyright: (Ray & Mackinnon, 2010))

2.3.1 Direct Repair

Direct repair is also called neurorrhaphy, which can be classified into three types of repair: epineurial repair, grouped fascicular repair and fascicular repair. Epineurial repair bridges two nerve ends by suturing the external epineurium so as to achieve good co-aptation of the proximal and distal fascicular anatomy. This clinical method helps the connective tissue to connect from the proximal to the distal stump without tension and with proper alignment. Grouped fascicular repair is used for those cases where one part of the cross section of the nerve supplies sensory function and another portion supplies motor function which can be easily distinguished. In some situations, the nerve injury

requires a split repair, in which the regenerating nerves are preserved in continuity, while the non-regenerating nerves undergo neuroorrhaphy. Fascicular repair is used for specific trauma situations where individual motor and sensory fascicles can be identified and need to be repaired separately (Griffin et al., 2013).

2.3.2 Autografting

When direct repair cannot be performed, nerve grafting is the current gold standard for treatment of peripheral nerve injuries. The time between injury and surgical treatment significantly affects the success of the reconstruction of the peripheral nerve, especially for young patients (Matejka, 2002). This is because the robust regenerative capacity of young patients facilitates the process of regeneration. Autografting provides neurotrophic factors and Schwann cells to help the axon to regenerate (Ray & Mackinnon, 2010). The time for regeneration of an axon to reach its denervated target is determined by the chronic denervated Schwann cells within the distal nerve stump particularly, when the time is longer than a month. For example, the regenerative rate of growth of an axon is reported to be 1 mm/day (Gordon, Sulaiman, & Boyd, 2003).

An autograft is often applied under tension, and in all cases nerve grafts should be at least 10% longer than the injured gap. The selected autograft tissues are usually sural nerves. Also, medial and lateral cutaneous nerves in the forearm and other parts of the peripheral

nervous system are possible choices. Noncritical portions of an injured nerve can be good choices for autografts so as to avoid the morbidity of the donor site. However, the question of morbidity at the donor site of the whole nervous the system are still critical concerns for autografts. The sutures that are used for secure the proximal and distal anastomoses may result in unfavorable fibroblastic proliferation, which will inhibit the development of the tiny axons (Merolli, 2009). In addition, the cost is higher for a double operative procedure involving both the donor and injured sites.

2.3.3 Neural Scaffolds

A potential alternative approach to autografting, which avoids the problem of morbidity of the donor site, is the use of a nerve conduit or nerve guide tube between the proximal and distal stumps. In addition, such nerve conduits have the advantage of available for immediate use when autografts are not readily available and they also serve the function as a barrier to scar tissue infiltration (Santin, 2009). Nerve conduits can bridge a longer nerve gap and may facilitate the collection of local neurotrophic factors. The application of nerve conduits is mainly for the reconstruction of small diameter sensory nerves with gaps of up to 30 mm. These scaffolds can either be biodegradable or non-biodegradable. The three main materials used to make bioabsorbable conduits are collagen, polyglycolic acid (PGA) and polycaprolactone (PCL). In Section 2.4, the use of biodegradable materials as nerve conduits is discussed further.

2.3.4 Allografts

The function of allografts is similar to that of autografts but avoiding the problems of short supply and donor site morbidity. Allografts can repair nerve gaps of up to 50 mm. However, successful reconstruction relies on the viability of both host and donor Schwann cells. The donor Schwann cells work both as support cells for remyelination and as facultative antigen presenting cells. Therefore, the main concern for using allografts is the side effect of immunogenicity (Ray & Mackinnon, 2010).

2.4 Biomaterials for Nerve Regeneration

For the biomaterials used to make a conduit for nerve regeneration, they must be able to not only direct the emerging axon sprout from the proximal to the distal stump but also prevent infiltration of the fibroblasts from the outside environment and allow cells to migrate and proliferation inside the tube. In addition, the artificial nerve guide should have the proper mechanical strength, flexibility, compression resistance and biocompatibility. The following resorbable polymers are widely used for nerve guide conduits: polylactic acid (PLA, "Neurolac" Ascension USA – Polyganics NL) (Figure 2.6), polyglycolic acid (PGA, "Neurotube" Synovis USA), polylactic-co-glycolic acid (PLGA), polycaprolactone (PCL) and Type I collagen ("NeuraGen" Integra USA)(Figure 2.6) (Merolli, 2009; Vroman & Tighzert, 2009).

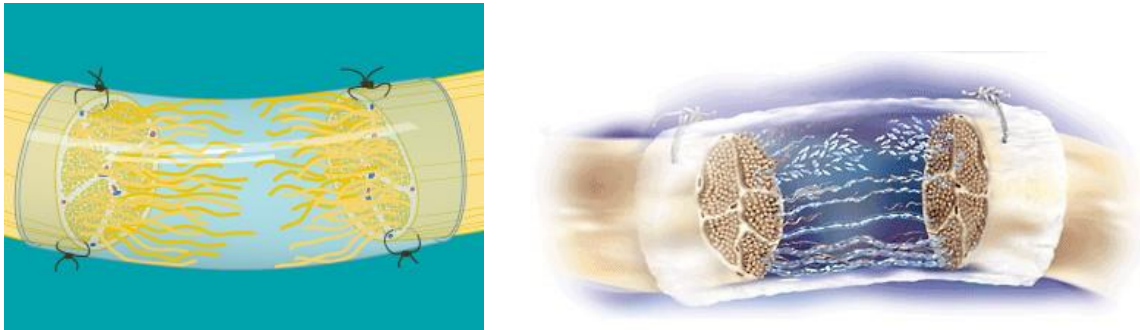


Figure 2.6 Commercial nerve guide conduits

(a) "Neurolac" Polyganics NL

(b) "NeuraGen" Integra USA)

(Copyright: (Polyganics, 2014a))

(Copyright: (Integra LifeScience Corporation, 2010))

2.4.1 Polylactic acid (PLA)

PLA is a green polymer, which can be manufactured from renewable agricultural resources, for instance, corn, potato, sugar cane and beets instead of non-renewable resources. The synthesis of PLA is usually through ring opening polymerization (ROP) after dimerization of lactic acid or by polycondensation (PC) of lactic acid (Figure 2.7 (a)) (Ratner, Hoffman, & Schoen, 2012). The monomers for polylactic acid (PLA) have two stereoisomeric forms: D-lactic acid or L-lactic acid (Figure 2.7 (c)). Therefore, two optical isomers exist for PLA: poly (L-lactide) (PLLA) and poly (D-lactide) PDLA. Also, the combination of different enantiomers exists such as poly (D, L-lactide) (PDLLA) and the mixture of PLLA, PDLA and PDLLA (Figure 2.7 (d))(Maharana, Mohanty, & Negi, 2009).

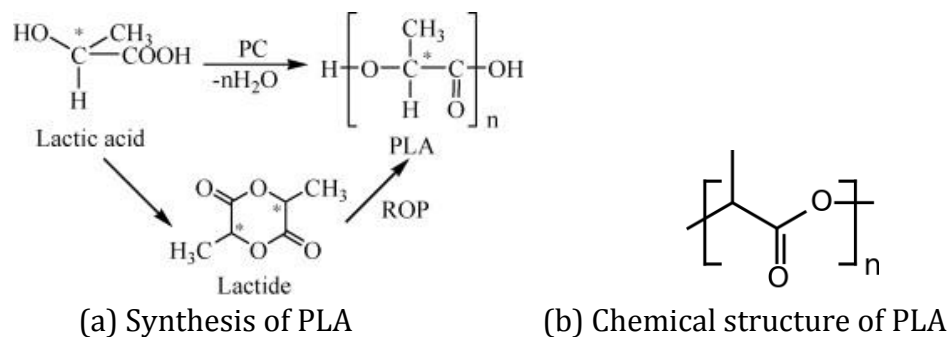


Figure 2.7 (a-b) Synthesis, chemical structure of PLA

(Copyright: (Maharana et al., 2009))

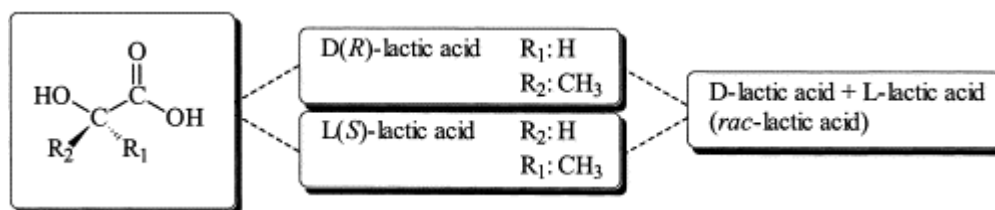


Figure 2.7 (c) Stereoforms of lactic acid

(Copyright: (Södergård & Stolt, 2002))

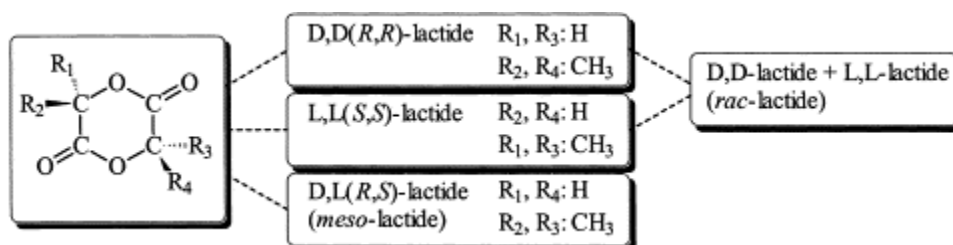


Figure 2.7 (d) Stereoforms of lactide by ring-opening polymerization

(Copyright: (Södergård & Stolt, 2002))

Although PLA is a hydrophobic polymer due to its methyl side groups ($-\text{CH}_3$), but it can be degraded into water and carbon dioxide through hydrolytic, enzymatic and microbial activity in marine and other environments. The semicrystalline PLLA has the tensile strength at break of 45-70 MPa and an elongation of 85%-105%. For some typical commercial PLLA products, the glass transition temperature is 63.8 °C and the tensile strength is 32.2 MPa with the elongation at break of 30.7% (Briassoulis, 2004). By increasing the molecular weight, the mechanical properties of crystalline PLLA show significant improvement. However, PDLLA is always an amorphous polymer. PDLLA is usually used for drug delivery where a homogeneous dispersion is required, whereas PLLA is often used for an application that requires high mechanical properties, such as sutures. Since the hydrolysis of PLLA yields only L-lactic acid, it is more widely used than PDLLA (Perego, Cella, & Bastioli, 1996). For the peripheral nerve repair, PLA conduits or PLA composite conduits (such as with chitosan) have been shown to be preferable materials for both commercial products and research (J. Liang, 2013; Xie, Li, Gu, Liu, & Shen, 2008).

2.4.2 Polyglycolic Acid (PGA)

Polyglycolic acid or polyglycolide (PGA) is a linear polyester with a highly crystalline (45-55%) structure. This leads to its high melting point (220-225 °C) and low solubility in organic solvents (Ratner et al., 2012). Its glass transition temperature is 35-40 °C. (Merolli, 2009). It is an absorbable polymer with excellent mechanical properties. Also,

when it degrades through hydrolysis of the ester group in the backbone chain, the aqueous byproducts are readily excreted from the body (Chandra & Rustgi, 1998). In addition, during the degradation process, acidic by-products are released. PGA was first used as a synthetic suture. However, it degrades so quickly that the suture loses its mechanical properties in 2 to 4 weeks after implantation. In previous research of nerve regeneration, PGA nerve guides have been shown to repair nerve injuries with up to 30 mm gaps with comparable results to autografting (Mackinnon & Dellon, March 1990).

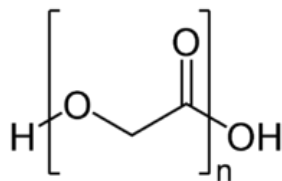


Figure 2.8 Chemical structure of PGA

(Copyright: (Mackinnon & Dellon, March 1990))

2.4.3 Polylactic-co-glycolic Acid (PLGA)

Poly (lactide-co-glycolide) (PLGA) was developed as an alternative to PGA. It is copolymerized by combining L-lactide and DL-lactide with glycolic acid monomer (Vroman & Tighzert, 2009). Although PGA is highly crystalline, the crystallinity of the copolymer, PLGA, is much lower than both PGA and PLA. Different ratios of the DL-lactide monomers and glycolic acid monomers (L/G) influence the degradation rate of the copolymer. The higher ratio results in a slower degradation rate. The copolymer PLGA

has been approved by the FDA for human use, and nanoparticles of PLGA are widely used for drug delivery therapies (Astete & Sabliov, 2006). Recent research found that PLGA fibers in the ratio of 75:25 promotes migration of axons and 85:15 improves growth of Schwann cells to support the peripheral nerve repair (Quigley, A. F., Bulluss. K. J., etc, 2013).

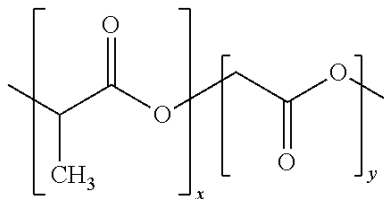


Figure 2.9 Chemical structure of PLGA

(Copyright: (Emanuel, Neuman, & Barak, 2004))

2.4.4 Poly (ϵ -caprolactone) (PCL)

Poly (ϵ -caprolactone) (PCL) is a nontoxic, non-immunogenic and biodegradable semicrystalline polymer in the family of aliphatic polyesters. It is synthesized by ring opening of ϵ -caprolactone (Figure 2.10). The glass transition temperature of PCL is relatively low, around $-60\text{ }^{\circ}\text{C}$ and the melting point is in the range of $59\text{-}64\text{ }^{\circ}\text{C}$ (Ratner et al., 2012). The modulus of PCL falls in the range between low-density and high-density polyethylene. Its tensile strength is 23 MPa and the elongation at break is more than 700% (Vroman & Tighzert, 2009). In a short term study, PCL conduits have demonstrated the feasibility to bridge a 10 mm nerve gap (Sun et al., 2010). In a longer term in vivo study of 18 weeks, the PCL nerve conduit showed equivalent results as autologous nerve

repair for a 10 mm nerve gap (Reid et al., 2013). PCL is widely used as an electrospun fibrous mat for nerve regeneration. Electrospun PCL/collagen conduits have also been shown to have the potential as an alternative clinical therapy for use in an end-to-side neurorrhaphy technique (Lee et al., 2012). An in vitro study has indicated that electrospun PCL results in superior nerve regeneration and mechanical properties, especially when the structure is oriented or aligned (Ciardelli & Chiono, 2006; Prabhakaran et al., 2008; Yao & O'Brien, 2009). In addition, caprolactone can be copolymerized with lactic acid to form poly(DL-lactide- ϵ -caprolactone), (PLC). VIVOSRB® is a bioresorbable polymer sheet for end-to-end nerve repair that claims to prevent neuroma formation (Polyganics, 2014b).

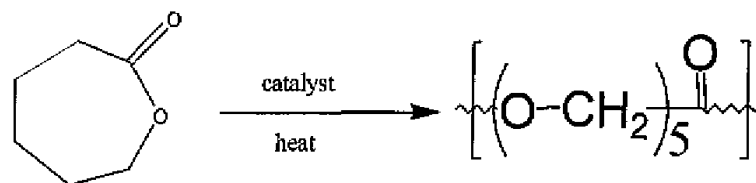


Figure 2.10 Chemical synthesis of PCL

(Copyright: (Hedhli, 2011))

2.4.5 Type I Collagen

Collagen is composed of various polypeptides and is the essential protein component in animal connective tissue (Vroman & Tighzert, 2009). It is usually found as extracellular matrix (ECM) protein to provide a natural environment for nerve regeneration (Bennet & Kim, 2011). An artificial nerve guide coated with collagen has demonstrated acceptable

biocompatibility and good mechanical properties. For example, an animal study has demonstrated that a double layer polyurethane-collagen nerve guide with collagen as the inner layer showed superior nerve repair results than the control group without collagen. This indicates the potential for collagen coated biomaterials in clinical applications for peripheral nerve repair (Lee et al., 2012; Wang & Cui, 2009). In addition, the collagen-blended chitosan nerve guides showed better functional repair and muscle strength repair when evaluated by a functional gait analysis technique (Patel et al., 2008). Collagens can be grouped into two different subfamilies, such as fibrillar collagens and non-fibrillar collagens. Type I collagen is a classical fibrillar collagen and it exists mostly in mammals (Fratzl, 2008). It provides the mechanical stability and strength for a range of different soft tissues from tendons to skin (Gevorkian, Allahverdyan, & Gevorgyan, 2013). NeuraGen® (Integra™, USA) is a semi-permeable, Type I collagen tube for peripheral nerve repair (Integra LifeScience Corporation, 2010). This product promotes the proliferation of Schwann cells and the extension of axons. Animal trials have found that the nerve regeneration results of NeuraGen® equal direct suture repair, and the presence of the collagen tube lasts three to four years in vivo. Integra™ also states that no scar tissue or inflammatory response was observed in their studies.

2.5 Carbon Nanotubes (CNTs) for Nerve Regeneration

2.5.1 Properties of Carbon Nanotubes (CNTs)

Carbon nanotubes (CNTs) were first discovered by Sumio Iijima in 1991 (Mishra, 2012). They are structurally part of the fullerene family and are basically allotropes of carbon composed of graphene sheets, which are one-atom-thick layers of graphite sheets rolled into hollow tubes (Figure 2.11). The length of a CNT can be up to several millimeters long, while the diameter of a nanotube is nearly $1/50,000^{\text{th}}$ of the width of a human hair. The chemical bonding of CNTs is by sp^2 bonds, which are similar to those of graphite and stronger than the sp^3 bonds found in diamond. The sp^2 bonds provide unique strength to CNTs. In addition, CNTs have the superior thermal conductivity and thermal properties.

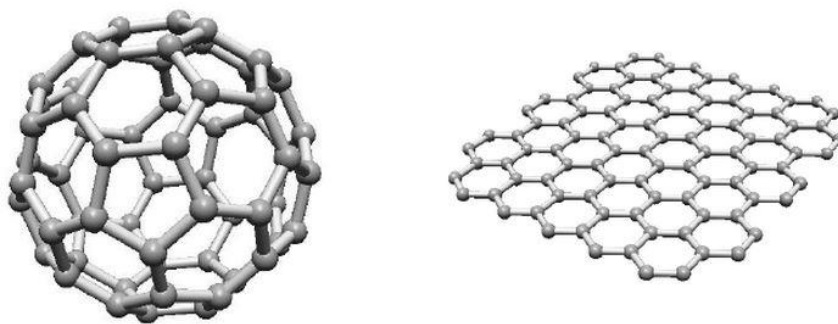


Figure 2.11 (a-b) Structure of fullerene and graphene

(a) Fullerene structure

(b) Graphene

(Copyright: (Mishra, 2012))

CNTs are categorized into two main groups: single-wall carbon nanotubes (SWNT) and multi-wall carbon nanotubes (MWNTs), according to the number of layers of graphene sheets. Single-wall nanotubes (SWNT) have a very small diameter, close to 1 nanometer, but with a length of millions of times longer. The structure of a SWNT can be fabricated by wrapping graphene into a hollow cylinder. The way of wrapping is represented by a pair of indices (n, m) (Figure 2.12 (a)). Different combinations of n and m significantly influence the properties of the SWNT. Both n and m are integers and they represent the number of unit vectors in the two directions of the two dimensional graphene sheet (Mishra, 2012). If $m=0$, the SWNTs are zigzag nanotubes; if $n=m$, they are armchair nanotubes; if n is not equal to m and m is not equal to 0, the nanotubes are in chiral shape. The electrical conductivity of SWNTs is similar in behavior to metals or semiconductors and the band gap of the SWNTs can be varied in the range of 0 to 2 eV. Note that SWNTs are much more expensive than multi-walled nanotubes (MWNTs). MWNTs consist mainly of multiple layers of rolled graphene sheets (Figure 2.12 (b)).

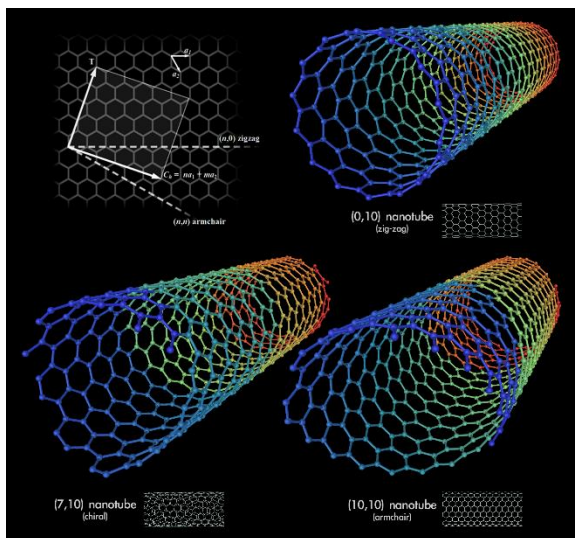


Figure 2.12 (a) Structures of SWNTs determined by the indices n and m

(Copyright: (Poore, 2007))

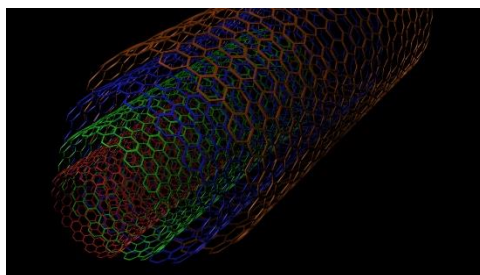


Figure 2.12 (b) Structure of MWNTs

(Copyright: (Young & The nanotechnology age, 2014))

The chemical reactivity, electrical conductivity, optical activity, mechanical properties and thermal properties of CNTs are all related to their one dimensional structures. Since CNTs are without functional groups, their chemical reactivity is determined by the π -orbital mismatch and curvature-induced pyramidalization. As a result, an enormous

strain is engendered by the curvature of the structure, which induces the reactivity (Niyogi et al., 2002). The graphene sheets of CNTs determine their conductivity. The different geometries of CNTs also determine the electrical behavior. Each carbon nanotube is unique and the relationship between their structure and electrical properties is highly correlated. The degree of helicity may determine the metallic or semiconducting behavior of SWNTs, but the metallic or semiconducting nature of MWNTs is also influenced by interlayer interactions (Ebbesen, Lezec, Hiura, & Bennett, 1996). CNTs are flexible, but their high Young's modulus in the axial direction allows them to withstand pressures of up to 24 GPa. Their strength is determined by the force of the covalent sp^2 bonds. The thermal conductivity in the axial direction at room temperature of SWNTs is similar to that of copper and similar to other conductive metals in the transverse direction. CNTs also have excellent thermal stability, and can withstand up to 2800 °C in vacuum and 750 °C in air.

2.5.2 Synthesis of CNTs

Four different methods have been developed and used to synthesize CNTs. Arc discharge was the first method used by Iijima in 1991 for CNTs fabrication (Mishra, 2012). The equipment involved establishing an electrical discharge between two graphite water-cooled-electrodes at high temperature (above 1700 °C) in a chamber full of helium under subatmospheric pressure. The second method involves laser ablation by utilizing lasers

to ablate a block of pure graphite. This is especially effective for fabricating SWNTs with high purity. The third method is flame pyrolysis, in which carbon nanotubes are created during the process of combustion. Parameters such as temperature, catalysts particle concentration, setup, and the type of flame and fuel influence the length, purity and diameter of CNTs produced.

Chemical vapor deposition (CVD), especially catalytic chemical vapor deposition (CCVD) is the fourth method, which lends itself to large scale production of CNTs. In this process, the feedstock of carbon monoxide or a hydrocarbon is heated to 800-1000 °C. The preferred carbon source is a hydrocarbon, such as methane, ethane or ethylene. The substrate is prepared with metal catalyst particles, such as Fe, Co or Ni. The catalyst in CVD is used to decompose the carbon source and create the CNTs. With the use of plasma enhanced CVD (PECVD), one can produce vertically-aligned nanotubes (Meyyappan, Delzeit, Cassell, & etc, 2003). The plasma is generated by an electrical field, which directs the growth of the CNTs. In this process, the precursor is first diffused through a thin boundary layer to the substrate, followed by adsorption of species on the surface. This surface reaction results in the growth of a film followed by the CNT product species being desorbed. Finally, the CNT species are diffuse through the boundary layer into a bulk stream.

2.5.3 Toxicity of CNTs

Thanks to the unique properties of CNTs, such as chemical, electrical and mechanical properties, CNTs have the potential to be used in biomedical applications and some research has been done to fabricate tissue engineering scaffolds with CNTs, such as nerve guides and drug delivery system. The toxicity of CNTs is related to many factors and there is not a standard systematic understanding of CNT toxicity (Liu, 2013). However, the CNT-based three dimensional (3D) matrices, such as 3D scaffolds are believed to reduce the toxicity of CNTs because the matrices resemble the natural extracellular matrix (ECM) (Serrano, 2014). In addition, it has been shown that limited doses of hydrophilic CNTs, such as 100 $\mu\text{g}/\text{mL}$ for MWNTs can be excreted through the urinary system without any toxicity (Serrano, 2014).

2.5.4 CNTs for Nerve Regeneration

Recently, nanomaterials, such as carbon nanotubes have been applied to the field of neuroscience. It is believed that on account of their conductivity CNTs could help in the growth and migration of neurons (Huang et al., 2012). In a recent research study, Huang et al fabricated a rope substrate made by twisting SWNTs together following synthesis by CVD. The rope had a diameter of 1 mm and a length of 15 mm. Neural stem cells were cultured on the CNT rope with electrical stimulation of 5 mV and 0.5 mA. The electrical stimulation was found to increase the rate of neurite growth and enhance the neuronal

maturity during the early stage of culture (Huang et al., 2012). In addition to SWNTs, MWNTs have also been shown to increase the neuronal adhesion and promote cell differentiation (Fabbro A et al., 2013). Composites and combinations of CNTs with other materials have also demonstrated experimentally improved neurite growth. For example, a chitosan/collagen composite incorporating CNTs, CNTs and chitosan fibers coated with laminin, a MWNT coating on a PCL scaffold, poly-L-lysine (PLL) coated CNTs, a silk/SWNT/ fibronectin nanocomposite and a MWNT-pHEMA composite have all been used for peripheral nerve regeneration (Arslantunali, Budak, & Hasirci, 2014; Huang YC et al., 2011; Jang MJ et al., 2010; Jin GZ et al., 2011; Mottaghitalab F, Farokhi M, & etc, 2013; Zhao et al., 2014). An electrospun collagen/PCL nerve conduit enhanced by MWNTs has also been tested in vivo and shown to have good biocompatibility and promote nerve regeneration (Yu et al., 2014). It has been proposed that CNTs may improve the hydrophilicity, mechanical properties and ease of degradation of nerve conduit. The adhesion and proliferation of mouse fibroblast cells on CNT samples has demonstrated their non-cytotoxic effects (Zhao et al., 2014). In vitro test results of PC-12 cells have shown that composites with CNTs encourage neurite out growth (Huang YC et al., 2011; Jin GZ et al., 2011). Other studies have indicated that the inclusion of Schwann cells contributes to the successful application of CNT composite in peripheral nerve regeneration (Mottaghitalab F et al., 2013). Also, the immune response has been evaluated by culturing human dendritic cells on MWNTs and a low immunogenic profile was found (Aldinucci, Turco, & etc, 2013). Human embryonic stem cells (hESCs) were

cultured on silk/CNT composite scaffolds, and the results confirmed that neuronal differentiation of hESCs took place. This indicates that the scaffolds containing CNTs may provide a unique opportunity for the treatment for spinal cord injuries (Chen et al., 2012).

CHAPTER 3

MATERIALS AND METHODS

3.1 Fabrication of Nerve Guides

The structure of the prototype nerve guides includes three major components: (i) braided inner PLA tube, (ii) aligned CNTs in a nonwoven structure and (iii) braided outer PLA tube. The steps in the fabrication process to make these prototype samples is shown in Figure 3.1.

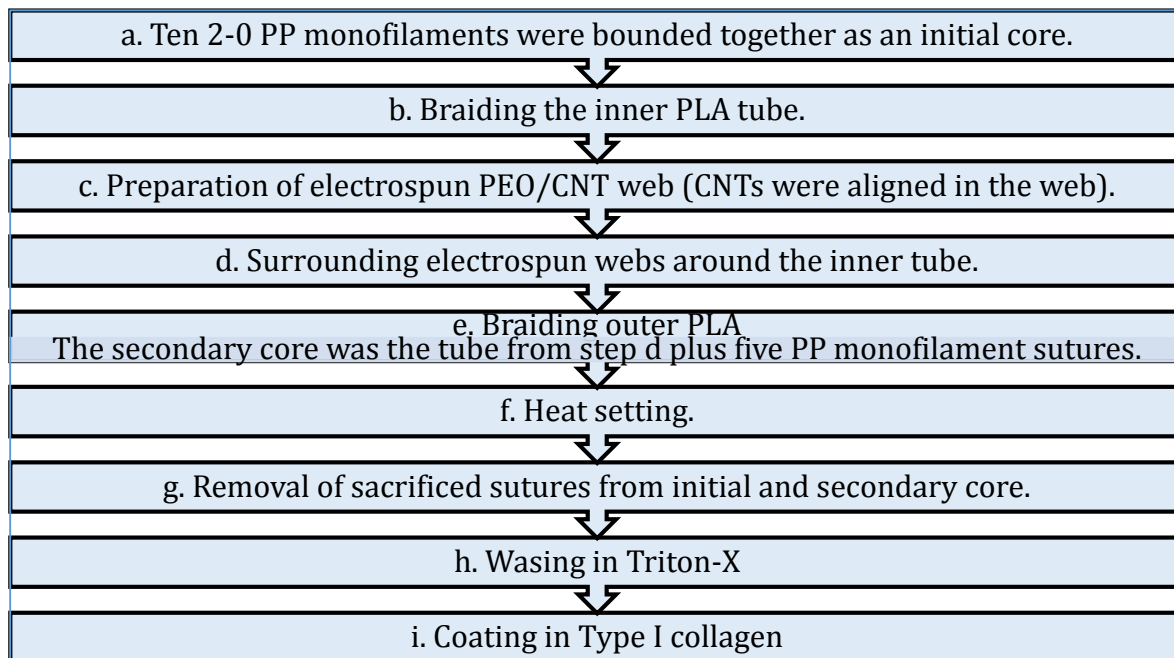
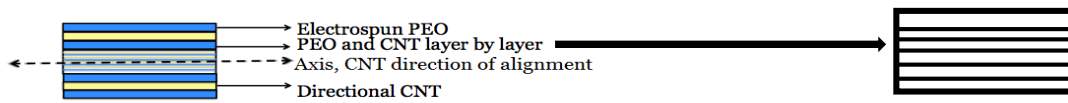


Figure 3.1 Flow chart of fabrication process

3.1.1 Preparation of Electrospun Poly(ethylene oxide) and CNTs

A forest of oriented MWNTs was fabricated as a composite with electrospun poly(ethylene oxide) (PEO). PEO is usually in the form of a non-toxic polyether diol, which is readily soluble in aqueous environment and the degradation byproducts can be eliminated by the renal and hepatic pathways (D. Liang, Hsiao, & Chu, 2007). Electrospinning is a unique technology to spin a non-woven mat of nanofibers on the conductive collector under a strong electrostatic field. Electrospun nanofibers have a high surface-to-weight ratio that can improve the extent and rate of single cell layer attachment. In addition, the electrospun PEO/CNT composite has good flexibility. This flexibility of permits the wrapping and plying electrospun PEO/CNT webs on the outside of inner PLA tubes. The solvent system for electrospinning PEO can be either ethanol, dimethylformamide (DMF), or chloroform and water (Son, Youk, Lee, & Park, 2004). In the current study, a 5% PEO solution in distilled water was electrospun and collected on a parallel array of MWNTs (Figure 3.1). Three types of electrospun webs were prepared: (i) 100 layers of electrospun PEO/CNTs, (ii) 200 layers of electrospun PEO/CNTs and (iii) electrospun PEO with no CNTs.



(a) Structure of electrospun PEO/CNTs (b) aligned CNTs (black straight line) on electrospun PEO (white)

Figure 3.2 Structure of electrospun PEO/CNTs

3.1.2 Braiding Nerve Guides

The total nerve guide fabrication procedure was divided into four sequential steps: winding, braiding, wrapping and braiding again. First, polylactic acid (PLA) yarns (FOY 170 den/18 filaments) were wound onto 16 small bobbins on the winding machine (Model: MS-888-SER.NO. 60). The winding time for the machine was 500 yards in 3 minutes or 167 yards per minute. Second, in order to braid a hollow structure, ten sacrificial 2-0 polypropylene (PP) black monofilament sutures each around 0.34 mm in diameter were laid parallel together as a core to make the nerve guide with internal diameter of 1.5 mm (J. Liang, 2013). They were subsequently removed prior to testing. The sutures were wound on 10 small bobbins and inserted into the braiding machine together through the central column so as to provide a central core structure (Figure 3.2(a)). Then 16 small bobbins were installed on the 16 spindles of the Steeger braiding machine (Type: K80/16-2008-SE) (Figure 3.2 (b)). The inner PLA tube was then braided with the machine set at 36 picks/inch and braiding speed of 150 rpm.



(a) Ten 2-0 PP black monofilament sutures wound on small bobbins ready to provide a central core. (b) 16 spindle Steeger braiding machine

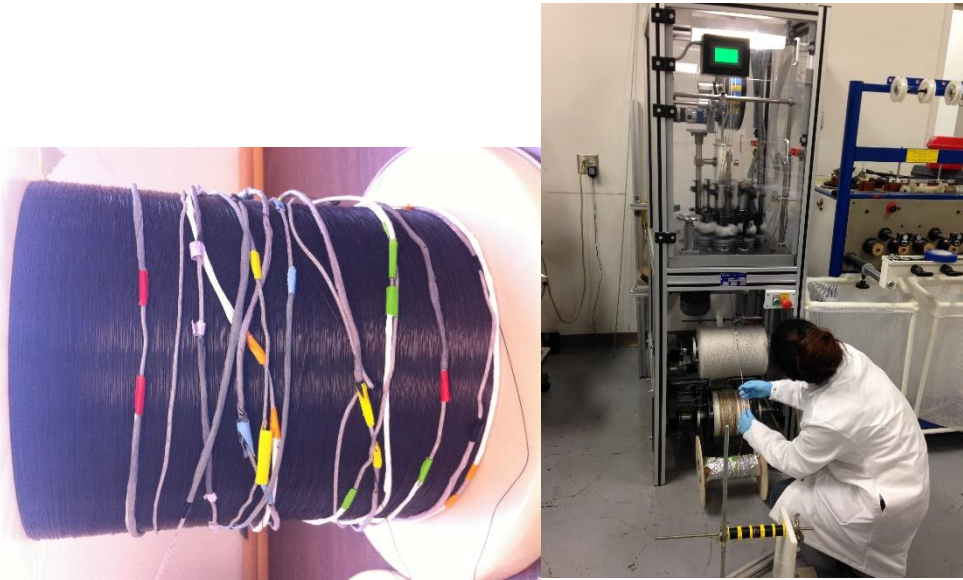
Figure 3.3 (a-b) Central core and braiding machine

After braiding the inner layer of the nerve guides, the PLA tube was thoroughly washed in 0.5% Triton-X at 30 °C to remove any oils and particle contamination that has been added to on the PLA tubes during the in braiding process. The inner PLA tubular layers were then dried at room temperature overnight.

The third step involved wrapping four different types of electrospun webs around the braided inner PLA layer of the nerve guides. They were (i) an electrospun PEO web, (ii) a 20 layer electrospun PEO/CNT web, (iii) a 40 layer electrospun PEO/CNT web and (iv)

a control group with no electrospun web. Five layers of each of the first three types of web were wrapped around the inner PLA layer. Different colored labels were used to distinguish the samples from each other (Figure 3.3 (a)).

In the fourth step, the inner PLA tubular layers with different webs wrapped around them were combined with five more 2-0 PP black monofilament sutures as to provide the space for growing cells. These four different types of composite tubular structures were then used as the central core during the braiding of the second outer PLA tubular layer (Figure 3.3 (b)). The braiding pick count of the outer layer was set at 48 picks/inch, which was different from the pick count of the inner tube. These different pick count settings led to different densities and porosities from the inner and outer tubular layers.



(a) Test specimens of inner PLA layer surrounded by CNTs aligned in the axial direction

(b) Five additional 2-0 PP monofilament combined with the inner PLA layer and electrospun webs being fed as a core into the central column of the braiding machine

Figure 3.4 (a-b) Second central core and second braiding process

3.1.3 Post Processing

Because the nerve guide final product was designed to be hollow with space for cell infiltration between the inner and outer layers. The 15 PP black monofilament sutures needed to be removed from the two layer composite tubular structure. So in order to prevent the two layer PLA tube from unraveling or distorting during the process of monofilament removal, the braided nerve guides with their internal cores were first heat treated. Different types of samples were cut at the length of 150 mm according to the color tapes. The heat setting condition was 80 °C for 2 minutes, which is above glass

transition temperature of PLA. After pulling out all the PP monofilaments (Figure 3.4(a)), the final multiple nerve guides were washed by 0.5% Triton-X at 30 °C for 4 hours and rinsed with deionized water three times. After they were dried overnight at room temperature, they were coated with 0.01 % Type I collagen (Soluble from calf skin, C806, Elastin) in 0.01 M acetic acid for 6 hours at room temperature and dried overnight. Therefore, the four sample groups were: (i) PLA nerve guide with 20 layers of PEO/CNT, (ii) PLA nerve guide with 40 layers of PEO/CNT, (iii) PLA nerve guide with electrospun PEO web only and (iv) control group of PLA nerve guide with no additional web (Figure 3.4(b)).

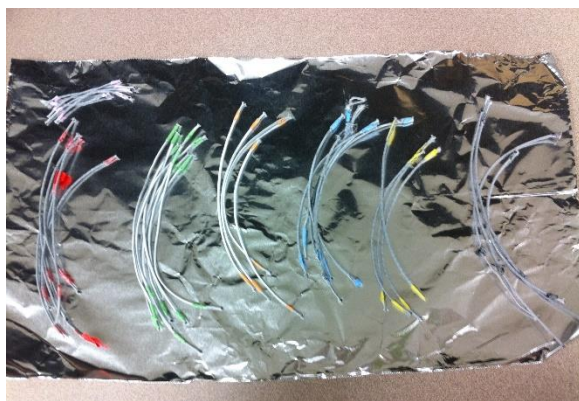


Figure 3.5 (a) View of specimens after pulling out black PP monofilament sutures

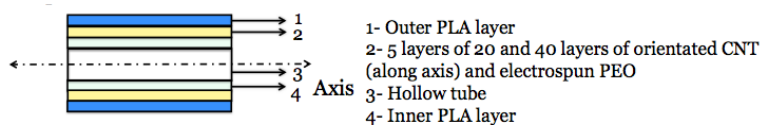


Figure 3.5 (b) Braided structure of final nerve guides

3.1.4 Total porosity and pore size

According to ASTM F2450-10 (Standard Guide for Assessing the Microstructure of Polymeric Scaffolds for Use in Tissue-Engineered Medical Products), the determination of porosity is the “ratio of void volume to total volume of a porous material and is often expressed as a percentage”. The total porosity of the nerve guide without CNTs could be calculated from the following equation according to ASTM F2450–10 (Standard Guide for Assessing Microstructure of Polymeric Scaffolds for Use in Tissue-Engineered Medical Products):

$$\text{Total porosity (\%)} = (1 - d_s / d_{\text{PLA}}) \times 100,$$

Where d_s is the density of nerve guide and d_{PLA} is the density of the PLA polymer. The density of PLA polymer is assumed to be 1.24 g/cm^3 (J. Liang, 2013). The density of each nerve guide was calculated from the mass divided by ten the average of cross-sectional area of a 10 mm long nerve guide:

$$d_s (\text{g/cm}^3) = m/V,$$

Where m is the mass (g) and V is volume (cm^3). The wall thickness of the outer tube was 0.13 mm and the wall thickness of the inner tube was 0.12 mm. The diameter of outer tube of the double layer nerve guide was 1.7 mm and the inner tubular layer was 1.3 mm from analysis by image J (Figure 3.5). So the volume of double layer tube can be calculated from:

$$\text{Volume (cm}^3\text{)} = (R_o^2 - r_o^2) \times \pi \times l + (R_i^2 - r_i^2) \times \pi \times l,$$

Where R_o is the outer radius of the outer tube, r_o is the inner radius of the outer tube, R_i is the outer radius of the inner tube and r_i is the inner radius of the inner tube. The ρ was 0.254 g/cm^3 for the control samples.

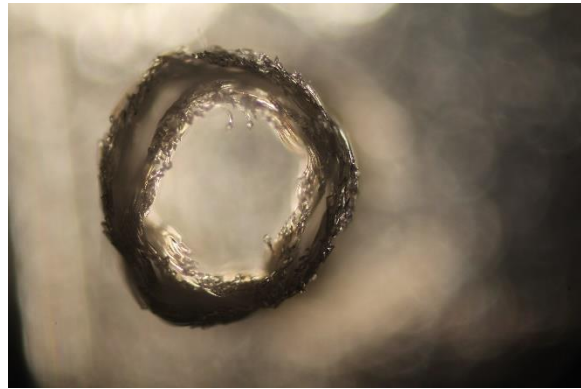


Figure 3.6 Cross section observed by microscope (4 \times)

According to ASTM F2450-1, pore size is the open space within a solid material. And in order to qualify the pore size one can apply a range of techniques, such as adsorption, X-ray scattering, electron microscope depending on the pore size. For pores measuring from 0.01 to $10 \mu\text{m}$, scanning electron microscope can be used to determine the average pore size and the pore size distribution. Therefore, the individual pore size of the inner layer tube and the outer layer tube was measured by scanning electron microscope. In addition, the distance between each CNT nanofiber was measured by a SEM image. 10 images of each group were taken, stored and analyzed.

3.2 Evaluation of Physical Properties of Nerve Guides

3.2.1 Tensile Strength and Elongation at Break

The standard tensile strength test (ASTM D 5035-11 Standard Test Method for Breaking Force and Elongation of Textile Fabrics) was followed using a crosshead speed of 300 mm/min and an initial gauge length of 30 mm. All nerve guide specimens were cut to a length of 60 mm to be long enough to be clamped in the top and bottom jaws. The maximum load, elongation at maximum load and elongation at break (or load drops by 80%) were recorded. Based on the above values, the Young's modulus was calculated for each specimen by determining the slope of the stress/strain curve during the first stage of the curve according to the following equation:

$$E = \text{tensile stress} / \text{tensile strain} = \sigma / \epsilon = \frac{F/A}{\Delta L/L}$$

Where E is Young's modulus (MPa), F is the absolute force applied on the tube (N), A is the cross-section of area of the tube, ΔL is the extension of tube in the axial direction (mm), and L is the original gauge length.

The tester was an Instron® mechanical tester, Model 2712-864 and the load cell capacity was 2 kN (Figure 3.6). The software for recording and analyzing the results was Bluehill 2 Material Testing Software. Five specimens were tested for each sample group.



(a) 60 mm long nerve guide specimens for tensile strength testing

(b) Tensile strength testing on the Instron® Model 2712-864 mechanical tester

Figure 3.7 (a-b) Tensile testing

3.2.2 Kink Resistance and Recovery

Kink resistance measurements were used to evaluate the ability of the nerve guides to maintain an open structure while being bent. In this test, the radius of curvature or kink resistance was measured when the nerve guide just started to kink or close during bending. The recovery of the nerve guides from kinking was evaluated by visually comparing the shape of the kinked nerve guide with the original shape (Figure 3.7). At least 3 specimens of were tested from each group (J. Liang, 2013).

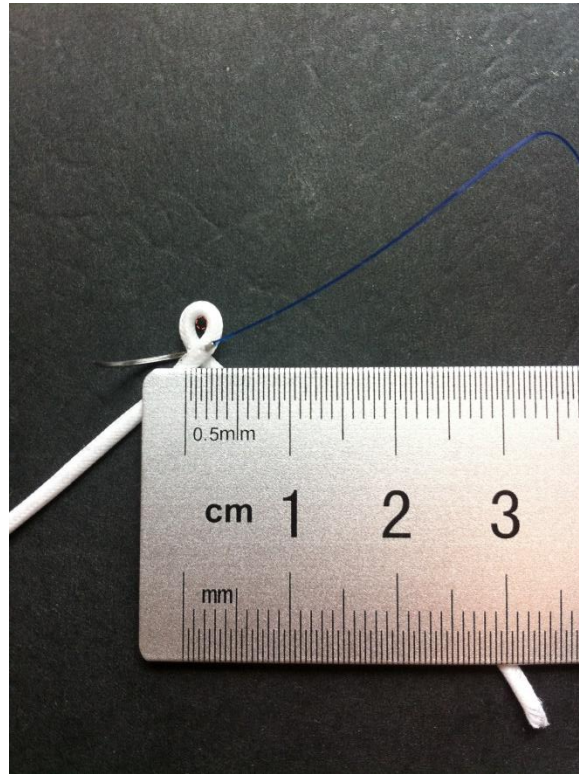


Figure 3.8 Kink resistance testing

3.2.3 Compression Resistance and Elastic Recovery

A compression resistance test was performed to evaluate the ability of the nerve guide to resist collapsing when under external pressure. The compression resistance was measured with a thickness gauge (SDL 94, Shirley Developments Ltd, Stockport, England) according to ASTM D6571-01 Standard Test Method (Determination of Compression Resistance and Recovery Properties of High Loft Nonwoven Fabric Using Static Force Loading) (Figure 3.8). During compression in the following loads: 20, 50, 100, 200, 700 and 1000g were applied incrementally to the top of each nerve guide. Delay of half-

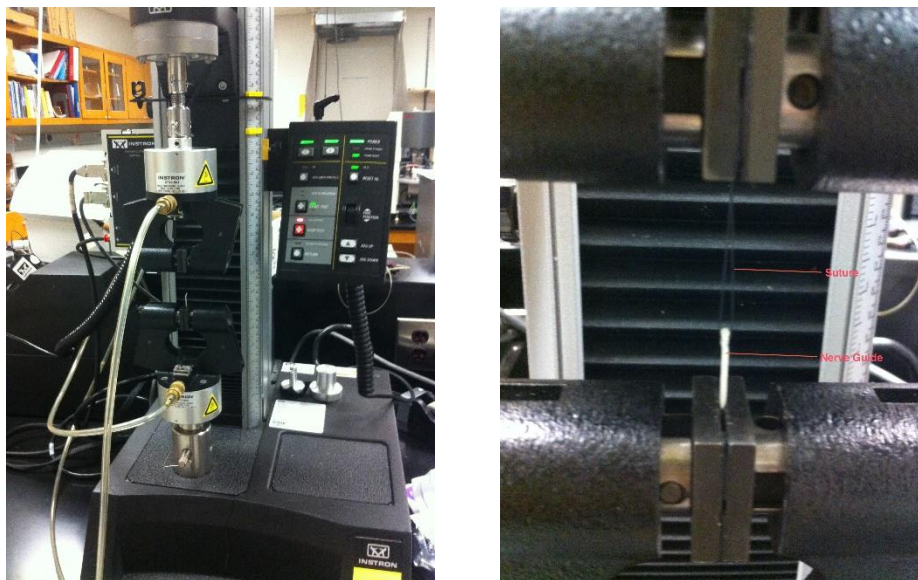
minute intervals were maintained between each incremental addition of load. At that point, the thickness value of the nerve guide was recorded. During the unloading cycle, the loads were unloaded over the same incremental range from 1000 to 20 g, with half-minute intervals between each thickness measurement. The thickness values at each load were then averaged, and the compression resistance was calculated as the thickness at each load. The elastic recovery was defined as the ratio of the final thickness at 20 g after compression and recovery divided by the thickness of initial 20 g before adding any load.



Figure 3.9 Compression resistance test

3.2.4 Suture Retention Strength

A suture retention test was performed so as to evaluate the resistance of pulling a suture out through the braided structure or causing the wall of the nerve guide to fail. In this test, a 20 mm cut length of nerve guide was mounted in an Instron[®] mechanical testing machine and a 2-0 black-braided nylon suture was passed through all the layers in the wall of the specimen at a distance of 2 mm from the cut end of the straightened nerve guide (Figure 3.9). The suture and one end of nerve guide were clamped in the tester (Figure 3.9). The crosshead speed was set at 200 mm/min (ISO 7198, International Standard of Cardiovascular Implants—Tubular Vascular Prostheses) and the break of nerve guide was defined as at least a 99% drop in load. The force for pulling out the suture or causing the wall to fail was recorded. Five specimens were tested for each group.



(a) Suture retention test on the Instron® testing machine

(b) Specimen set up



(c) Specimen preparation for suture retention test

Figure 3.10 (a-c) Suture retention testing

3.3 Biological Performances of Nerve Guides

3.3.1 Sample Preparation

All samples were cut down to 10 mm long specimens (Figure 3.10) and placed in a 24-well plate. Each nerve guide was put in a single well. Samples were sterilized with ethylene oxide overnight and kept in the hood for 48 hours so as to release remaining ethylene oxide. Then the specimens were immersed in 70 % ethanol for 15 minutes, followed by a 3 times PBS wash.



Figure 3.11 Nerve conduits at the length of 10 mm.

During sterilization procedure, only one nerve guide conduit at 10 mm in one well.

3.3.2 Preparation and Harvesting 3T3 Fibroblast Cells

The 3T3 cell line was obtained from embryonic fibroblast mouse cells (ATCC® CRL-1658, Lot 60731982). The complete culture media was composed of 89% DMEM (Dulbecco's Modified Eagle's Medium, 4,500 mg/L glucose) with phenol red, 10% CBS (Calf Bovine Serum, ATCC® 30-2030) and 1% PSS (Penicillin-Streptomycin Solution, Cellgro® 30-002-CI). The cells were unfrozen and prepared a week before culturing on the nerve guide samples. During procedure, aseptic conditions were strictly maintained. All vials, centrifuge tubes, flasks and other supplies were sprayed with 70% ethanol before use. Firstly, a T-75 flask with 15mL of complete culture media was incubated in 37 °C and 5% CO₂ for at least 15 minutes. Secondly, the frozen vial was thawed in a water bath at 37 °C for approximately 2 minutes. Then the vial was transferred to the hood and the contents were transferred to a sterile centrifuge tube with 9 mL of complete culture media, followed by centrifugation at 125 × g for 10 minutes. Finally, the supernatant liquid was discarded and the cell suspension was transferred to the prewarmed flask containing 15 mL of complete growth media.

When confluency had reached 80%, subculturing was required. First, the culture media was aspirated from the flask and the cells were washed 2 times with HBSS (Hanks' Balanced Salt Solution, Sigma H 6648). Second, 2 mL of 0.25% trypsin-EDTA (ATCC® 30-2101) was added to the flask and it was examined under an optical microscope confirm that the cells were detached. When the cells appeared to be detached, 8 mL of complete

culture media was added and the suspension was transferred into a sterile centrifuge tube. Then 15 mL fresh culture media was added to a new flask to allow the cells in suspension to be counted and their viability determined. This enabled the required number of cells to be transferred to a new flask with 15 mL of culture media. In fact, in order to obtain enough cells, two flasks were subcultured and the media was changed every three days.

3.3.3 Seeding 3T3 Fibroblast Cells on the Nerve Guides

The cells were obtained from the subcultured flasks three days before seeding. After counting the cells, a 20 μ L cell suspension with 10^4 cells was added to the tip of each 10 mm nerve guide in between the inner and outer layers. For these nerve guides that contained a CNT layer, the cells were seeded in the space between the inner layer and the CNT layer. In addition, each plate had cells seeded directly on the surface of the wells to serve as controls. After the cells were seeded, all 24-well plates were incubated at 37 °C and 5% CO₂ in an incubator for 20 minutes. Then 0.5 mL of culture media was pipetted into each well, and it was changed every second day.

3.3.4 Cell Proliferation by MTT Assay

Thiazolyl blue tetrazolium bromide is a water soluble salt yielding a yellowish solution, which is changed to an insoluble purple formazan when reduced by enzyme activity. This

MTT assay measures the number of viable cells present, and it was performed on Day 1, Day 3 and Day 7 of the 3T3 fibroblast cell culture experiment. 50mg MTT (thiazolyl blue tetrazolium bromide, Sigma M5655) were dissolved in 10 mL RPMI-1640 (Roswell Park Memorial Institute medium, Sigma R7509) without phenol red. The stock solution was sterilized through a 0.2 μm filter and stored at 2-8 $^{\circ}\text{C}$ in the refrigerator for frequent use and frozen at -20 $^{\circ}\text{C}$ in the freezer for long periods. The original media was removed and washed with PBS. The nerve guides were moved to new 96 well plates and 250 μL of fresh complete growth media (89% RPMI-1640, 10% Calf Bovine Serum, 1% Penicillin-Streptomycin Solution) was pipetted into the 96-well plates. 25 μL of MTT stock solution was added to each well. Then the plates were covered with aluminum foil to eliminate the light and incubated for at least four hours so as to have enough time to form the insoluble purple formazan. At the end of the incubation period the excess liquid was carefully aspirated without removing the purple crystals and leaving only about 25 μL of liquid in each well. Then 50 μL of DMSO (Dimethyl Sulfoxide, 25-950-CQC, Corning[®]) was added as an MTT solvent and the plates were incubated at 37 $^{\circ}\text{C}$ for 10 minutes covered with aluminum foil (lifetechnologies, 2014). Once the nerve guides had been removed, the intensity of the dye at absorbance of at 540 nm was measured in a Synergy (multi-mode) micro-plate reader. The background absorbance at 630-690nm was subtracted. The values of eight repeat specimens were averaged.

3.3.5 Live/Dead Proliferation and Migration of Cells by Laser Scanning Confocal Microscope

A live/dead assay was performed on the cells after culturing them on the nerve guides for days. 4 μM EthD-1 (Ethidium Homodimer-1) stock solution was prepared by adding 20 μL of 2mM EthD-1 to 10 mL sterile 1x DPBS (Dulbecco's Phosphate-Buffered Saline) and thorough by mixing by centrifugation. The experimental live/dead solution was diluted by adding 5 μL of 4 mM calcein AM to the 10 mL EthD-1 solution. This was then mixed thoroughly by centrifugation. Sample preparation for the live/dead was as following. First, the old media was removed from the 24-well plates. Second, each well was washed with 1x DPBS three times for 30 seconds, and the third wash was left in place. Third, 1.5 mL centrifuge tubes were prepared and labeled with 0.6 mL of the live/dead experimental solution. Fourth, the nerve guides were transferred in to the 1.5 mL centrifuge tubes and incubated for 20 minutes at room temperature, protected from the light. The nerve guides were separated into different components. Inner tube and CNT web were viewed separately. The whole length of the inner tube was viewed and the uniformity of cell distribution was assessed. Finally, the samples were mounted on the coverslips and viewed under a laser scanning confocal microscope (LSCM, Zeiss LSM 710). The wavelengths used are $\lambda_{\text{ex}}\sim 494$ nm and $\lambda_{\text{em}}\sim 517$ nm for the live cells, and $\lambda_{\text{ex}}\sim 528$ nm and $\lambda_{\text{em}}\sim 617$ nm for the dead cells.

3.3.6 Cells Attachment by Scanning Electron Microscope

The level of cell attachment to the nerve guides after 7 days of culture was evaluated by scanning electron microscope (SEM). The nerve guide samples after cell culture with cells were prepared for SEM as follows. First, any remaining liquid was decanted from the wells and washed with 0.1 M PBS at pH 7.4. Second, after the PBS had been aspirated the samples were fixed with 3.0% glutaraldehyde in 0.1 M PBS at pH 7.4 and 4 °C for at least 48 hours. Third, then each well was washed with 0.1 M PBS at pH 7.4 three times each for 30 minutes at 4 °C. Fourth, the nerve guides were dehydrated in a series of graded ethanol solutions for 30 minutes each solution at 4 °C. The solutions had 30%, 50%, 70%, 95% and 100%. Following this dehydration procedure immersion in a second and third 100% ethanol solution was performed at room temperature for critical point drying. Critical point drying was undertaken in a critical point dryer (Samdri®-795) for 15 minutes (Figure 3.11 (a)). After mounting the samples on stubs with carbon tape they were sputter coated with gold/palladium in a Hummer® Model 6.2 sputter coater (Figure 3.11(b)), The prepared nerve guides were in a desiccator and examined for cell attachment in a JEOL Model 5900LV scanning electron microscope using an accelerating voltage of 15 kV (Figure 3.11(c)).



(a) Critical Point Dryer



(b) Sputter Coater



(c) JEOL Scanning Electron Microscope

Figure 3.12 (a-c) Equipment for preparation and operation of scanning electron microscope

3.4 Statistical and Analysis

The means and standard deviations were calculated using a SPSS-22 (IBM) software program. The differences between the means of each group was analyzed by an analysis of variance (ANOVA) test. A one way, between groups, ANOVA was tested to compare the variance of the means for the four groups of nerve guide conduits. The p-value calculated during the ANOVA procedure tested the null hypothesis. If the p-value was ≤ 0.05 , then the difference between the group mean values was significant. Then the independent-samples t-test results were compared to find if there was a difference between the two individual group mean. If the p-value was ≤ 0.05 , then the null hypothesis was rejected and the difference between the two individual group means was found to be significant.

CHAPTER 4

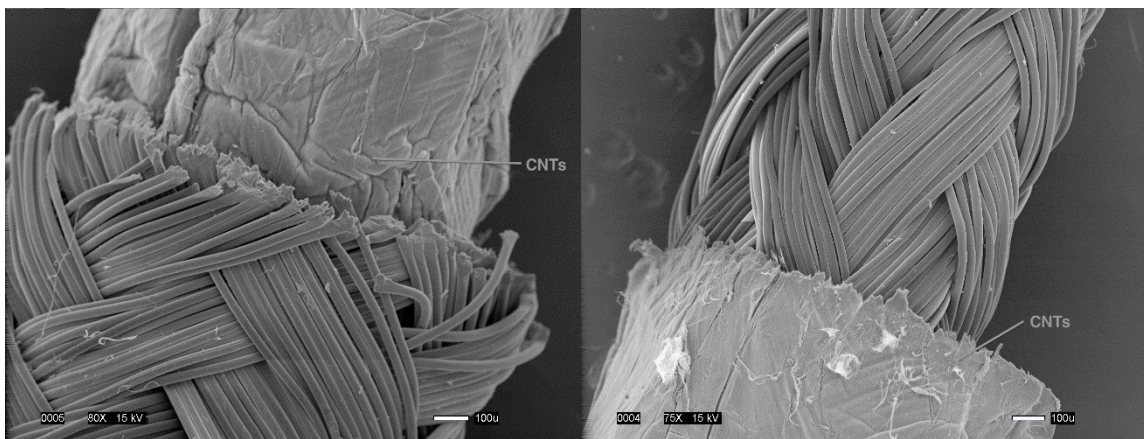
RESULTS AND DISCUSSION

4.1 Basic Properties of Multiple Layer Nerve Guides

4.1.1 Structure of Multiple Layer Nerve Guides

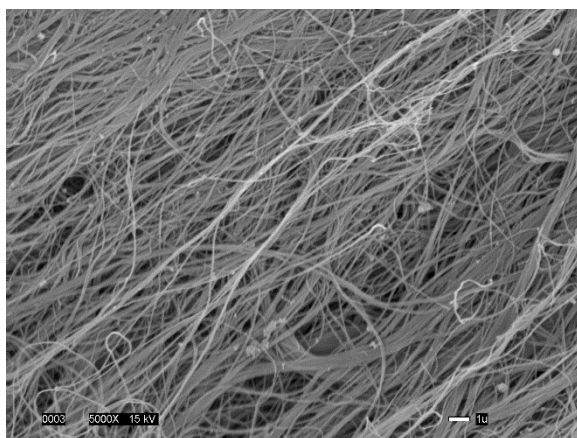
The nerve guide conduits were braided from PLA fully oriented yarns (FOY) (170 den/18 filaments) for both the inner and the outer tubular layers. Different prototype samples of nerve guide were fabricated by including the following unique features: (i) 100 layers of electrospun PEO/CNT webs, (ii) 200 layers of electrospun PEO/CNT webs, (iii) five layers of electrospun PEO without CNT and (iv) control samples containing only the inner and outer PLA tubular layers. The four samples were named: 100 CNT, 200 CNT, PEO, CONTROL. During the heat setting treatment process the PEO nanofibers melted and were washed away by the Triton-X surfactant, followed by washing thoroughly with deionized water. Therefore, the additional components in the 100 CNT and 200 CNT samples were aligned CNTs in between the PLA inner and outer layers (Figure 4.1). The SEM images show the internal structure of the nerve guide conduits containing CNTs. Also, the remaining components in the PEO sample were only the PLA inner and outer tubes once the sacrificial PEO layer had been washed away (Figure 4.1). However, the

heat setting treatment that melted the PEO layer may have influenced the physical and/or biological properties. This was the rationale for including the PEO sample as a control during the testing. The results will be discussed in this chapter.



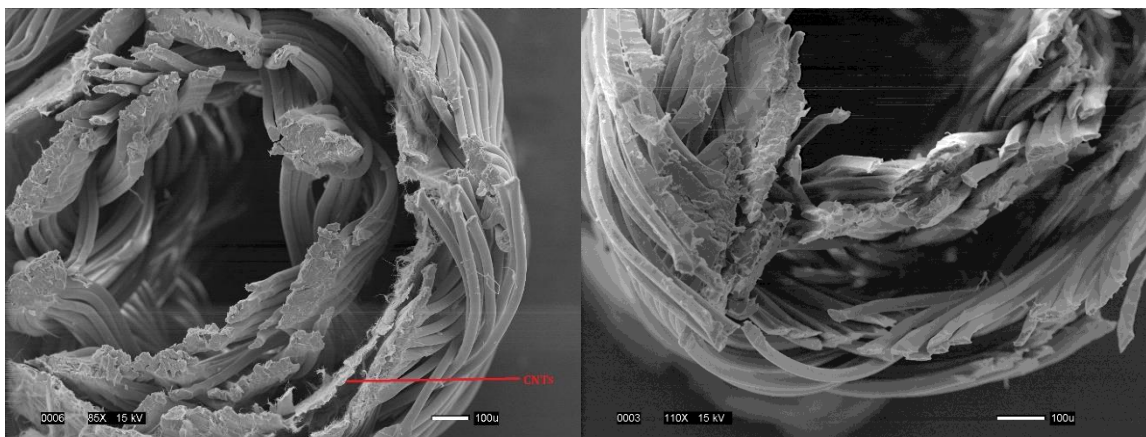
(a) CNTs and outer PLA tube (b) Inner PLA tube and CNTs on it

Scale bar: 100 μm .



(c) Web of CNTs under 5000x magnification. Scale bar: 1 μm .

Figure 4.1 (a-c) Images showing structure of 200 CNT sample.



(d) CNT layer in between the inner and outer PLA tube. (e) Only the PLA inner tube and outer tube remain for the PEO sample. Scale bar: 100 μm .

Figure 4.1 (d-e) Cross-sectional images showing structure of 200 CNT sample and PEO sample.

4.1.2 Braiding Parameters for the Braided Nerve Guides

The braiding angle θ was calculated using the following equation (General Cable, 2014):

$$\theta = \tan^{-1} \left| \frac{2\pi(D+2d)P}{C} \right|,$$

Where D is the inside diameter of the tube (inch), d is the diameter of the yarn (inch), P is the pick count (picks/inch) and C is the number of carries. After analysis by Image J software of the images taken by SEM and Optical Microscope, the average diameter of the inner tubes was 1.3 mm and for the outer tubes was 1.7 mm. The braided pick counts were designed to be 36 picks/inch for the inner tube and 48 picks/inch for the outer tube. The braiding machine was a Steeger 16 spindle braiding machine. This means it had 16

carriers. The above calculation gave a braiding angle of 36° for the inner tube and an angle of 51° for the outer tube. The SEM images were analyzed and compared with these theoretical values. The difference was about 5° , which may be due to the shrinkage of the PLA polymer during the heat setting process. It is known that different braiding angles can increase the compression resistance of nerve guide conduits (J. Liang, 2013).

After braiding, the thickness of the CNT layer was significantly reduced as a result of the heat setting treatment. The force during the braiding process was not as large as the pressure during heat setting. During the heat setting process, the PEO nanofibers melted and penetrated into the pores between the CNTs. In addition, as the PLA yarns reached its glass transition temperature, inner and the outer PLA tubes would be expected to shrink. This shrinkage would have resulted in increased pressure on the CNTs, which would have increased the density and reduced the thickness of the CNT layer. Table 4.1 presents the structural information of the different nerve guide prototypes.

Table 4.1 Braided structure for each nerve guide prototype

	Special layer in between the inner and outer tubes	Braiding Parameters		Thickness of CNT layer	
		Braiding picks/inch	Braiding angle	Before braiding	After braiding and heat setting
100 CNT	100 layer CNTs	Inner: 36 Outer: 48	Inner: 36° Outer: 51°	0.58mm	0.09mm
200 CNT	200 layer CNTs			1.15mm	0.12mm
PEO	None, electrospun PEO washed away			---	---
CONTROL	None			---	---

4.2 Physical Properties

4.2.1 Porosity and Pore Size

By applying the equation in Chapter 3: Total porosity (%) = $(1 - d_s/d_{PLA}) \times 100$, the total porosity of the PEO and CONTROL samples was calculated to be 77.2% and 79.5% respectively. The lower porosity for the PEO sample may have been due to the melting of the PEO, which contributed to additional nerve guide shrinkage over and above any shrinkage of the PLA polymer. For the composite nerve guide prototypes composed of

both PLA and CNTs, the total porosity were calculated by taking into account the percentage of each component:

$$\text{Total porosity (\%)} = [1 - (d_s/d_{\text{PLA}} \times P_1 + d_c/d_{\text{CNT}} \times P_2)] \times 100,$$

Where d_c is the density of CNTs web in the composite, d_{CNT} is the theoretical density of one carbon nanotube, P_1 is the weight percentage of PLA and P_2 is the weight percentage of the CNTs. The theoretical density of MWNTs is 2.1 g/cm^3 (Cheap Tubes Inc, 2014) and of PLA is 1.24 g/cm^3 (Liang, 2013). The pore size of each component in the four nerve guide prototypes was also measured and analyzed by Image J. Table 4.2 lists the results of total porosity and pore size for each sample.

Table 4.2 Total of porosity and average pore size for four nerve guide prototypes

	Total porosity	Pore size		
		Inner tube	CNT layer	Outer tube
100 CNT	76.9%	5-25 μm	0.5-1 μm	20-50 μm
200 CNT	74.5%			
PEO	77.2%		---	
CONTROL	79.5%			

Rutkowski found that the optimal total porosity of a nerve guide needed to be 75% so as to facilitate the growth of Schwann cells. Lower total porosity values reduced the permeability of growth factors and oxygen transference, whereas higher porosity nerve conduits are more likely to loose growth factors from the lumen, which shows the growth of axons (Rutkowski & Heath, 2002). The above calculations show that the addition of

CNTs reduced the total porosity of the nerve guide. The porosity of the 200 CNT sample was around 75%, which is an appropriate pore size for nutrient supply and oxygen exchange. However, the difference in total porosity between the 100 CNT and the PEO sample was not significant, possibly due to the small amount of CNTs added. The average pore size for the inner tube was in the range of 5-25 μm , which ensured nutrient exchange and prevented the loss of cells migrating through the wall. The average pore size of the CNT layer was between 0.5-1 μm . Given the small size of these pores, it is unlikely that they could provide a channel for nutrient exchange. However, note that the purpose of this study was to fabricate novel multiple layer nerve guides with CNTs and to ascertain whether or not they are cytocompatible. In future studies the CNTs will serve as core and the double layer PLA tubular structure will be braided around this CNT core so that the nutrients and oxygen can be readily transferred through the wall of the tubes.

4.2.2 Tensile Strength and Elongation at Break

Tensile strength of a nerve guide is important when practicing clinical surgery. Although the surgery of grafting nerve conduits involves careful handling, nevertheless some tension is still applied to the nerve guide at the time of surgery. In addition, the internal anatomical environment of the human body and the movement of muscles will apply additional tension to the nerve conduit. Table 4.3 shows the means of the tensile test results for each prototype sample in terms of the maximum load and the elongation at

break. Figure 4.2 (a) compares the average maximum load between the four samples, whereas Figure 4.2 (b) compares the average percent elongation at break values.

Table 4.3 Results of tensile strength

		100 CNT	200 CNT	PEO	CONTROL
Maximum load (N)	Mean	68.4	71.5	61.5	69.3
	S.D.	3.83	6.26	3.48	7.00
Elongation at break (%)	Mean	64.7	62.2	70.6	66.9
	S.D.	3.63	6.77	7.16	14.68

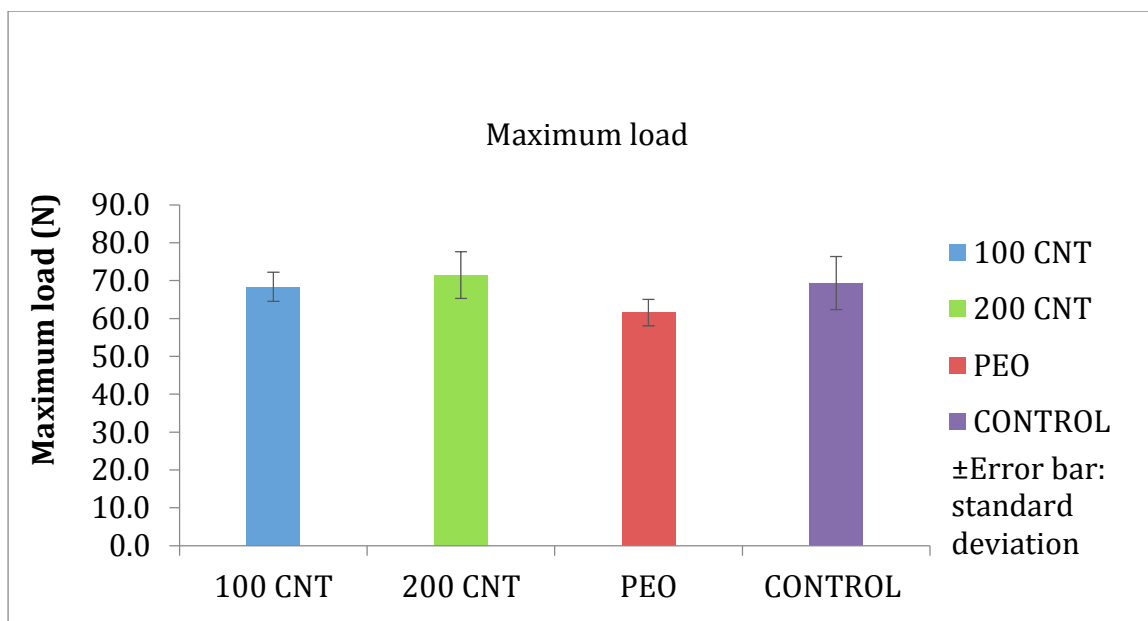


Figure 4.2 (a) Tensile strength results: maximum load

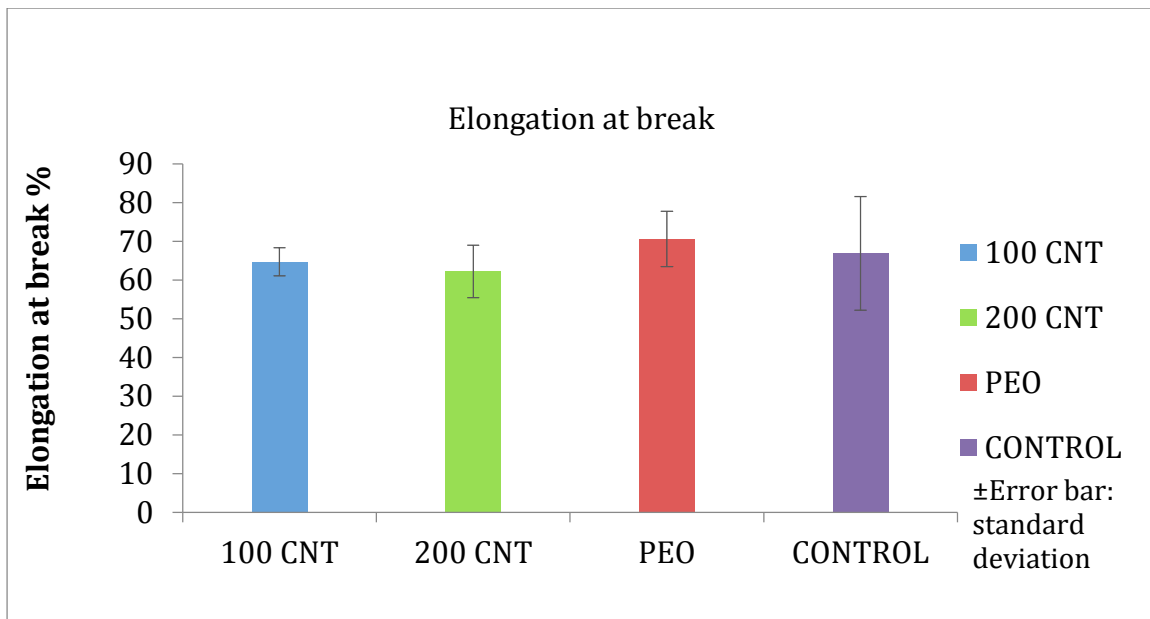


Figure 4.2 (b) Percent elongation at break

In order to determine whether the average tensile strength values between any of the four prototype samples were significantly different from the rest, it was necessary for the ANOVA statistical test to generate a 95% confidence interval where the $p\text{-value} \leq 0.05$. For the average maximum load, only the PEO sample gave a value significantly lower than the other three samples ($p\text{-value} \leq 0.05$). For percent elongation at break, no significant differences were found ($p > 0.05$). The difference in tensile strength between the high content CNTs and the low content CNTs was also found to be no significant ($p > 0.05$), which suggests that the amount of CNTs did not significantly influence the tensile strength of the nerve guide prototypes. The low tensile strength of the PEO sample may be due the additional imperfections in the two layer composite structure caused by the

melting of the PEO. Otherwise the presence of the CNTs generally increased the elastic modulus of the nerve guide. The curves in Figure 4.3 represent the typical load/elongation relationships for each sample as well as for the inner and outer PLA tubes, which were tested independently of each other.

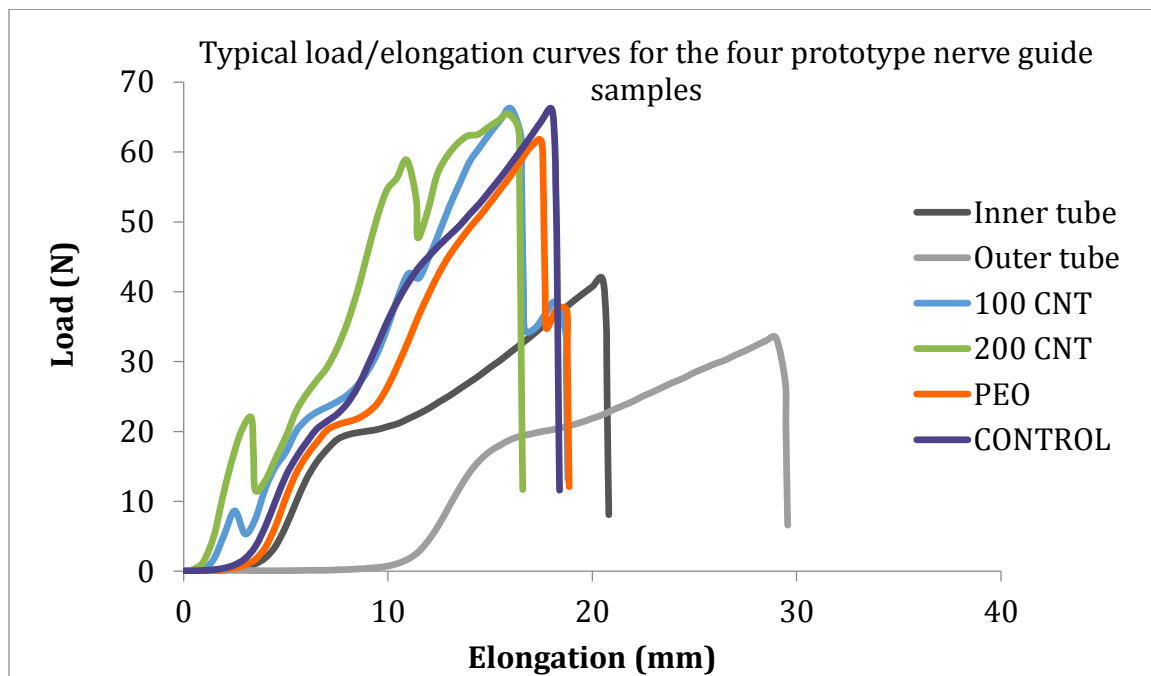


Figure 4.3 Comparison of load/elongation curves

In Figure 4.3, the nerve guides that contain CNTs show two peaks before reaching their maximum load. The slope during the initial stage is much steeper than for these samples without CNTs. This indicates that the nerve guides with CNTs have a higher modulus than these samples without CNTs. The first peak is most likely due to slippage of the CNTs

under tensile loading due to the applied tensile load being larger than the friction force between the CNT web and the inner PLA tubular layer. The second peak was most likely introduced by failure of the CNT layer. It is worth noting that the design of a double layer PLA nerve guide had a higher elastic modulus compared to the single layer either inner or outer prototype layer.

4.2.3 Kink Resistance and Recovery

Kink resistance is a crucial property for the successful performance of a nerve guide. If the kink resistance is low, the lumen of the nerve guide will close under limited bending and result in the inhibition of axon regeneration. Commercial nerve guides extruded as polymer tubes are rigid structures and they tend to kink when bent (J. Liang, 2013). Figure 4.4 shows the experimentally measured radius of curvature of the four nerve guide prototypes tested for kink resistance. The radii of the samples without CNT were significantly smaller than those with CNTs ($p \leq 0.05$) but little difference was observed between the 100 CNT and the 200 CNT samples ($p > 0.05$). The lower kink resistance may be influenced by the added stiffness of the CNTs. However, the radius of curvature for all the prototypes was smaller than 1 mm, which suggests that all four samples had excellent kink resistance.

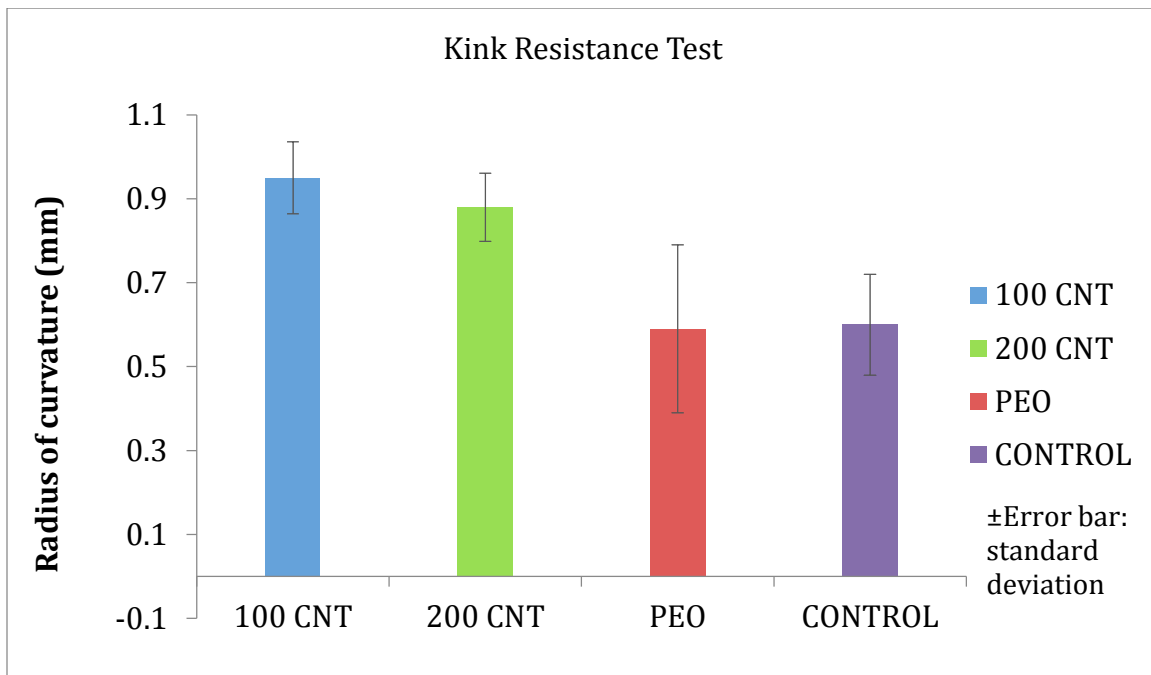
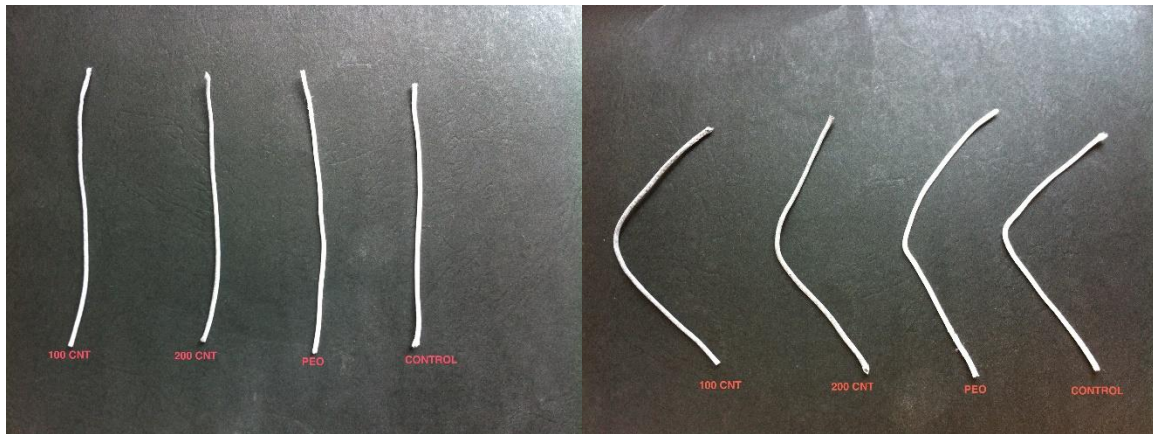


Figure 4.4 Kink resistance test

Figure 4.5 shows the images of the four prototypes before and after performing the kink resistance test. All four nerve guide samples recovered with an open lumen, which confirms acceptable kink recovery performance for all of the braided nerve guides, especially the ones with CNTs. This desirable kink resistance and kink recovery performance will ensure that the lumen of these nerve conduits does not close and reduce the space for axon of regeneration.



(a) Original prototypes

(b) kinking recovery after kinking

Figure 4.5 (a-b) Prototype nerve guide samples before and after kink resistance testing.

4.2.4 Compression Resistance and Recovery

When nerve guides are implanted in the human body, they will experience externally applied pressure from the surrounding tissue and liquid environment. The applied pressures in the body will vary over time due to normal daily activities, which will allow the nerve guide to recover from the compression. Therefore, the compression resistance and recovery are critical performance parameters for nerve guides to make sure they keep their shape and provide enough space in the lumen for axonal regeneration. As mentioned in Chapter 3, the compression test was undertaken by sequentially increasing and decreasing an applied external force in 30 s intervals. Table 4.4 gives the thickness results for the four different prototype nerve guides under specific external pressures.

Table 4.4 Results of radial compression and recovery testing

Force applied (g)	Thickness (mm)			
	100 CNT	200 CNT	PEO	CONTROL
20	0.78	0.85	0.78	0.92
50	0.57	0.57	0.47	0.61
100	0.46	0.48	0.36	0.46
200	0.40	0.41	0.32	0.39
500	0.34	0.34	0.26	0.31
1000	0.29	0.30	0.22	0.27
500	0.31	0.32	0.24	0.29
200	0.35	0.36	0.27	0.32
100	0.38	0.39	0.30	0.34
50	0.42	0.43	0.34	0.38
20	0.49	0.51	0.42	0.47

Figure 4.6 shows the changes in thickness under increasing and decreasing radial compression force as listed in Table 4.4. The slope of the PEO sample is the lowest, which indicates that the PEO nerve guide had the lowest compression resistance and compression recovery performance.

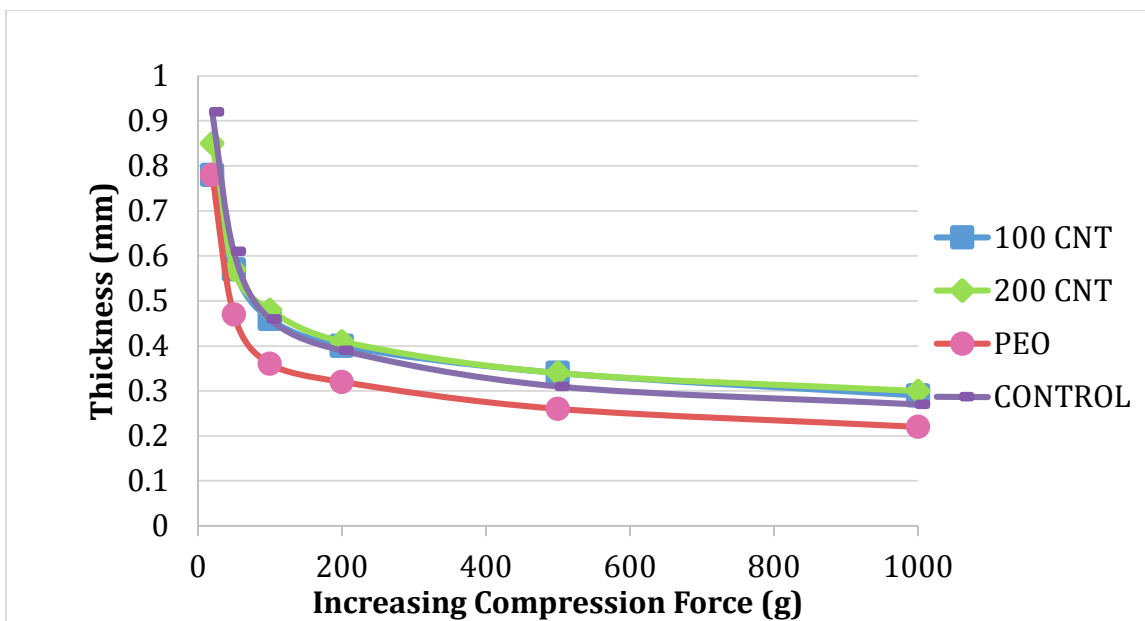


Figure 4.6 (a) Compression resistance test results

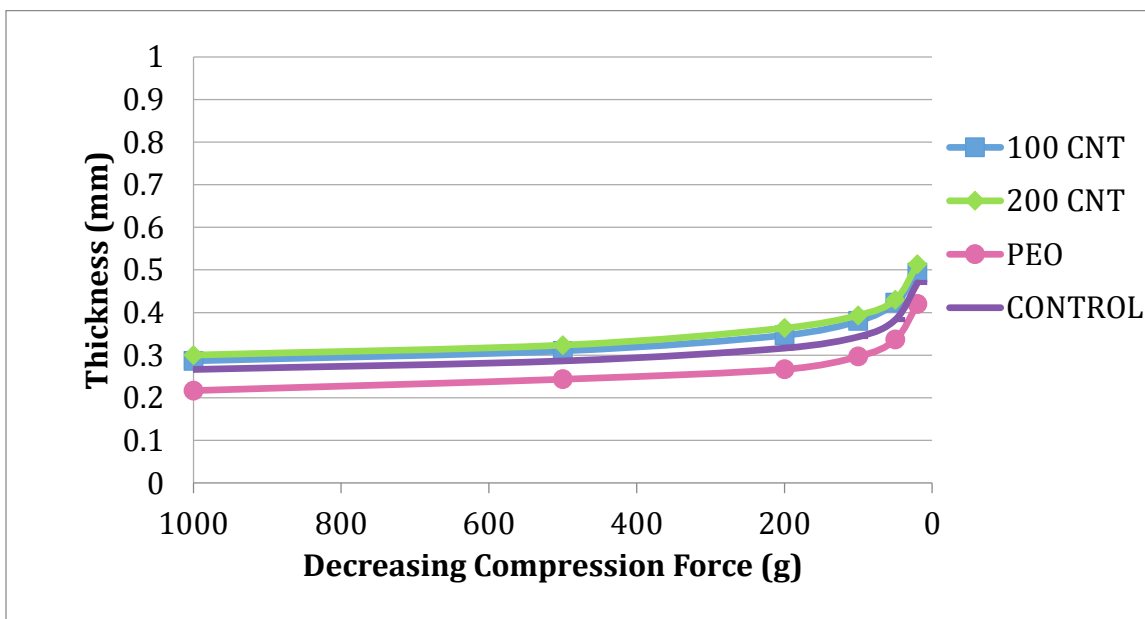


Figure 4.6 (b) Compression recovery test results

Based on the results in Table 4.4 and Figure 4.6, the overall level of compression resistance and compression recovery was been plotted in Figure 4.7. As mentioned in Chapter 3, the compression resistance was calculated from the thickness at the highest load divided by the thickness at the lowest load, and the compression recovery was obtained from the original thickness at 20 g divided by the final thickness at 20 g load.

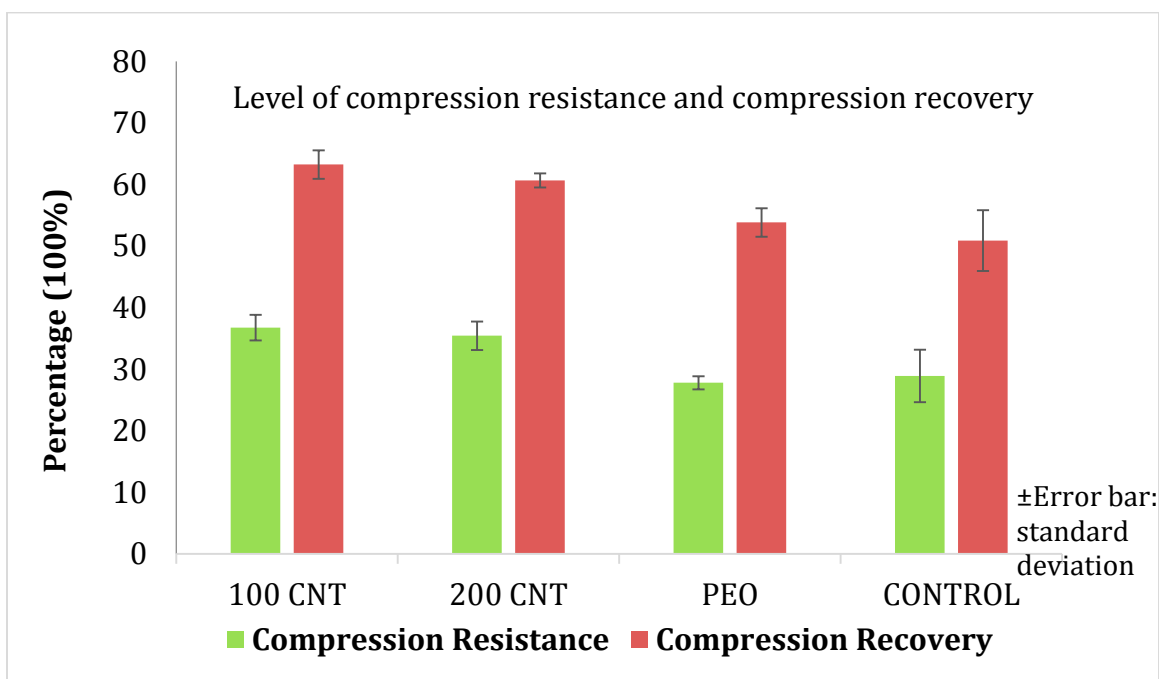


Figure 4.7 Comparison of the levels of compression resistance and compression recovery

The level of compression resistance for the two samples with CNTs is significantly higher ($p < 0.05$) than for the PEO and CONTROL samples. This is most likely due to the additional stiffness contributed by the CNTs. In addition, a similar significant difference was

observed in the compression recovery for the nerve guides with CNTs and the two samples without CNTS ($p \leq 0.05$). This points to the advantages of including CNTs in the nerve guides to improve their compression recovery. However, the p-values between the 100 CNT and the 200 CNT samples are larger than 0.05, which suggests that the amount of CNTs does not affect the compression resistance or the compression recovery. We therefore conclude that the inclusion of CNTs inside the nerve guides helps them maintain their shape and will facilitate axonal regeneration.

4.2.5 Suture Retention

During the grafting of nerve conduits the nerve guide needs to be attached to the proximal and distal injured and severed nerve stumps. This is usually achieved by suturing, which is a careful and delicate procedure (Birch, 2013). Even so, the requirement of suture retention strength for nerve guides needs to be sufficient to ensure long term attachment. Table 4.5 shows the average suture retention strength results for the four prototypes. The differences between the four samples are not significant ($p > 0.05$), which indicates that suture retention is largely determined by the braided structure, rather than the component materials for nerve guide (Figure 4.8).

Table 4.5 Results of suture retention strength

		100 CNT	200 CNT	PEO	CONTROL
Suture Retention Strength (N)	Mean	25.2	27.4	24.0	21.9
	S.D.	5.45	3.15	6.27	3.68

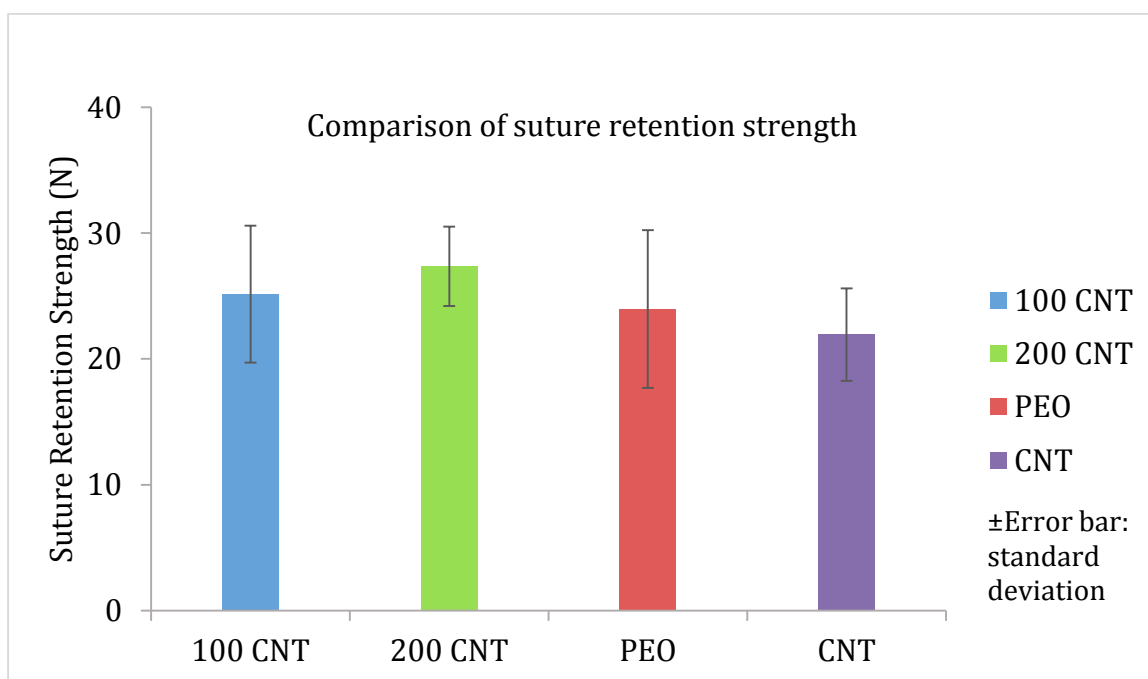


Figure 4.8 Comparison of suture retention strength

4.3 Biological Performance

4.3.1 Cell Viability and Proliferation by MTT Assay for Biocompatibility

The use of an MTT assay provides a method to measure the extent of cell viability and cell proliferation on the nerve guides. As mentioned in Chapter 3, the MTT assay was undertaken on Day 1, Day 3 and Day 7. The average and standard deviation of the absorbance results at 540 nm for these three days is listed in Table 4.6. Figure 4.9 shows the comparison between four prototypes on each of these three days.

Table 4.6 Absorbance percentage results from MTT assay

		100 CNT	200 CNT	PEO	CONTROL
Day 1	Mean	10.5	11.2	11.1	10.8
	S.D.	0.7	0.7	1.5	0.7
Day 3	Mean	18.3	19.9	22	19.9
	S.D.	1.7	2.8	5.1	0.9
Day 7	Mean	21.1	16.9	27.4	17.4
	S.D.	4.4	2.3	6.8	2.4

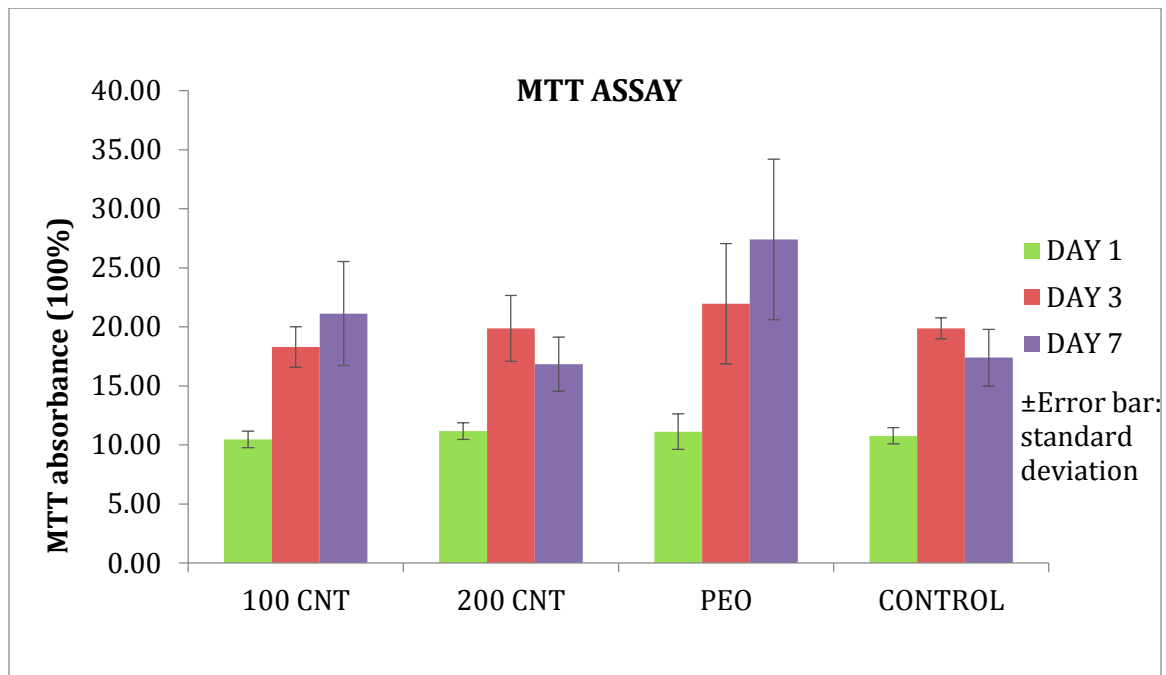


Figure 4.9 Results of MTT assay on Day 1, Day 3 and Day 7

For each of the prototype samples that extent of cell proliferation on Day 1 and Day 3 is significantly different ($p \leq 0.05$), which may be due to the fact that the cells had reached their maximum density which would have been either controlled by the limitation of space and/or by insufficient nutrient supply. The level of cell viability on Day 1 and/or Day 3 were the same for all four samples, whereas on Day 7 significant differences were observed in between some of the samples. For example, the MTT assay gave a significantly greater value for the 100 CNT sample compared with the 200 CNT sample ($p \leq 0.05$). This suggests that the higher content of CNTs may reduce the proliferation of 3T3 cells on nerve guides. This result may be introduced by the short distance between

inner PLA layer and the CNT web, which could not provide enough space for cell proliferation. It is therefore suggested that, in future studies, the space around the CNT be enlarged. The fall in proliferation of the 200 CNT and CONTROL samples on Day 7 may also be due to the overgrowth of cells. Note that there is no significant difference extent of cell proliferation on Day 7 between 100 CNT, PEO and CONTROL samples, which confirm that all four nerve guide samples had equivalent biocompatibility. Therefore, CNTs have the potential to be used in biomedical applications, especially in nerve guides for peripheral nerve regeneration.

4.3.2 Cell Migration and Proliferation of Live/Dead by LSCM

Another test method for determining the viability of cells is to use live & dead staining under a fluorescence microscope. The different wavelengths of the two components in the staining kit enable one to determine independently the live or dead activity of cells. If the cells are alive, they appear green under a fluorescence microscope. However, if the cells are dead, they give a red color. The live & dead images of all four prototype samples were taken on Day 7. As mentioned in Chapter 3, the fluorescence microscope used in the study was also a laser scanning confocal microscope (LSCM), which can focus at several different depths through the thickness of the nerve guides. Figure 4.10 shows the LSCM images of the CONTROL sample. The first three images were obtained separately named of the live cells, the dead cells and the PLA inner layer. They were then synthesized into

one image showing the live cells, dead cells and the PLA layer superimposed. In order to obtain a clear resulted view of the cellular performance, an images with only live cells and dead cells was generated using Adobe Photoshop (Figure 4.10 (b)). Figure 4.11 shows the superimposed images of the cells and the PLA layer on Day 7 for all four prototypes.

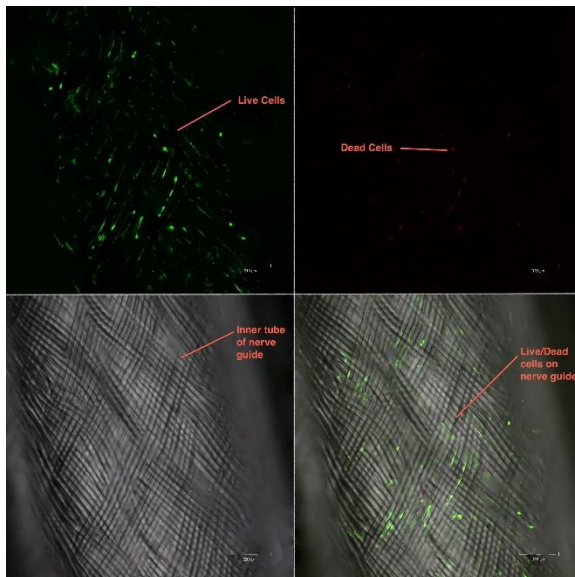


Figure 4.10 (a) Four images for the CONTROL sample on Day 7:

showing (i) only live cells (top left), (ii) only dead cells (top right), (iii) inner PLA layer without cells (lower left) and (iv) combined image showing live cells, dead cells on the PLA layer (lower right). Scale bar: 200 μm

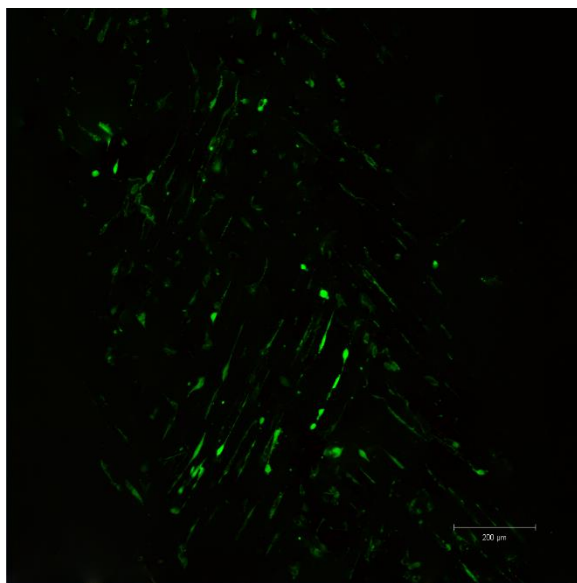
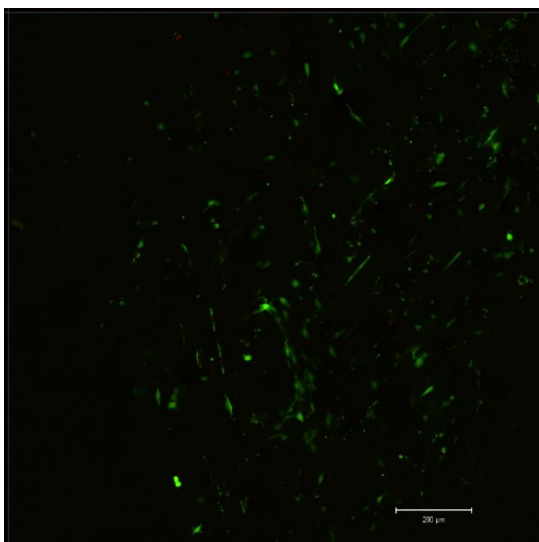
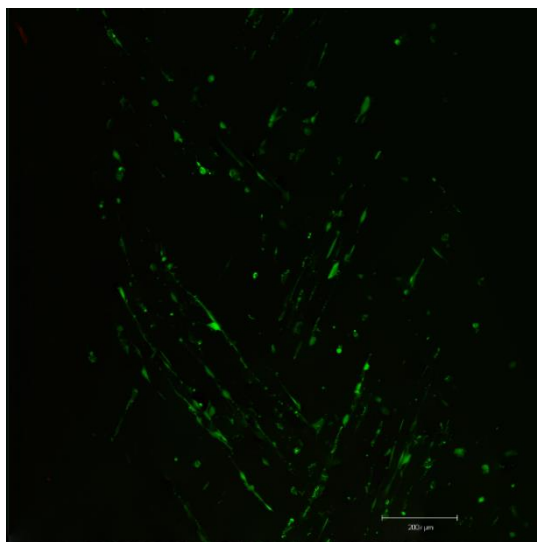


Figure 4.10 (b) Combined image of the CONTROL sample showing the live and dead cells without the PLA layer after Adobe Photoshop correction.

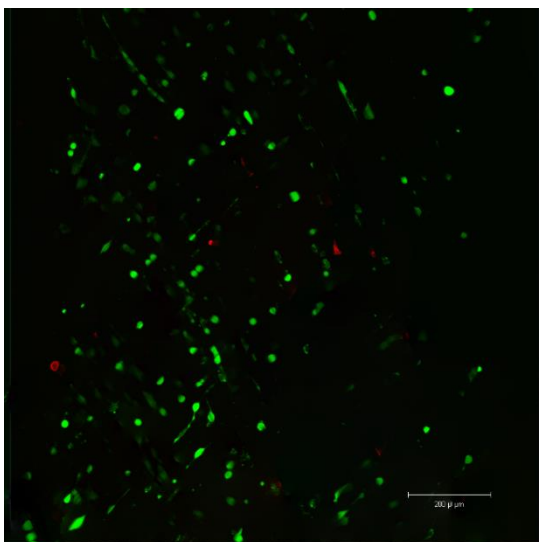
Scale bar: 200 μm



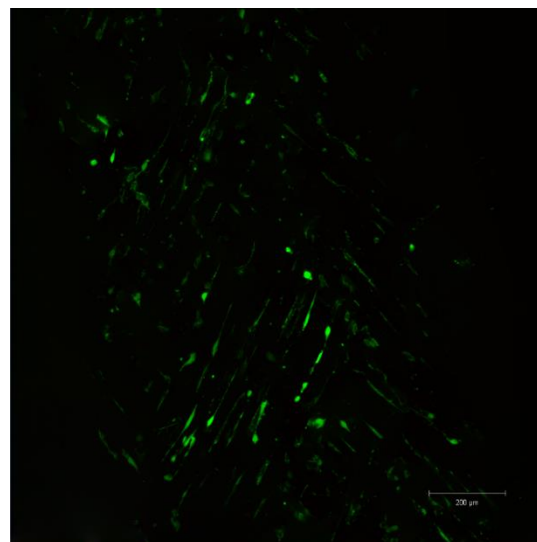
(a) 100 CNT. Scale bar: 200 μm .



(b) 200 CNT. Scale bar: 200 μm .



(c) PEO. Scale bar: 200 μm .

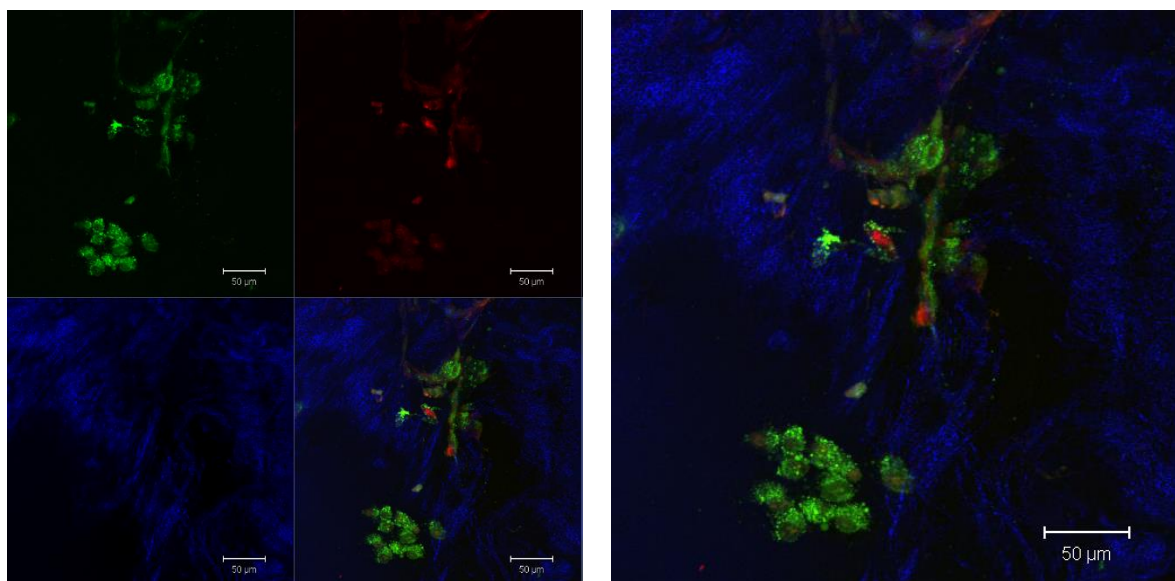


(d) Control. Scale bar: 200 μm .

Figure 4.11 (a-d) Live and dead cells on the inner PLA layer for the four different nerve guide samples on Day 7.

From the above four images, one can observe that most of the cells appear to be green, which indicates that the cells prefer to grow on the PLA layer. More cells grew on the PEO sample compared to the other prototypes which confirm the MTT assay result for the PEO sample on Day 7.

It is important to note that the cells grew along the yarn direction of the braided PLA tubes for all four nerve guide conduits and distribution of cells were the same along the whole length. This demonstrates that the biocompatibility of the PLA layer is acceptable and the structure of the braided nerve guides can promote the viability and migration of cells. The fact that the cells survived on the PLA inner layer reflect that the CNTs are non-toxic for the 3T3 cells. In order to demonstrate that the cells were attached to the CNTs, Figure 4.12 shows the images of live and dead cells on the 200 CNT prototype. Figure 4.12 (a) consists of four images combined together. In this figure, the blue represents the CNTs and the lower right image with three colors shows the superimposed view of the live cells, the dead cells and CNTs.



(a) Four images showing: Live cells (top left). Dead cells (top right). CNTs (bottom left). Combined image (bottom right). (b) An enlarged combined image. Scale bar: 50 μm .

Figure 4.12 (a-b) Images represent 3T3 cell viability on the CNTs on Day 7.

Both live and dead cells appeared to be attached to the CNTs, which agrees with the reduction in viability on the 200 CNT sample on Day 7. This reduced proliferation of 3T3 cells may be due to the limited space between PLA inner tube and the CNTs and the small pore size of the nanotube web, which would have inhibited nutrient exchange. In the future, the CNTs should be incorporated as a core layer inside the inner PLA tube and braided with a larger number of removable monofilaments so that the space between them will be significantly enlarged. In addition, this will avoid the disadvantage of the small pore size in the CNT web that limits nutrient and oxygen exchange.

4.3.3 Cell Attachment of SEM

While the live/dead cell assay illustrates the viability of the cells, the attachment of cells to the nerve guides needs to be demonstrated by an alternative technique. Eventually Schwann cells will have to attach themselves and grow along the nerve guides so that the axons can regenerate. In this study, SEM three dimensional images were taken to show the attachment of the 3T3 cells on the nerve guides. Figure 4.13 shows the cell attachment of 3T3 cells on both the CNTs and the PLA yarn layer.

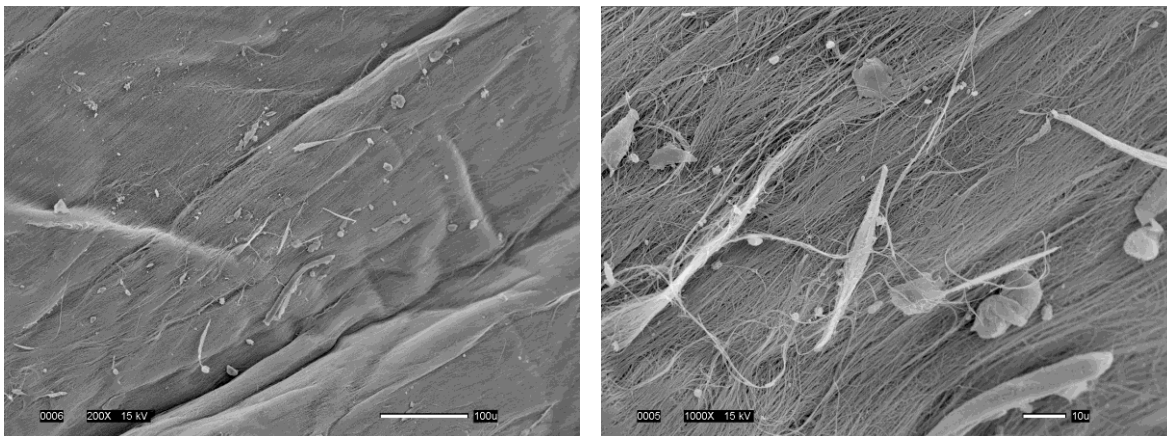


Figure 4.13 (a) Cells attached to the CNT web of the 100 CNT sample

Figure 4.13 (b) Cells attached to the CNT web of the 100 CNT sample.

Scale bar: 100 μm .

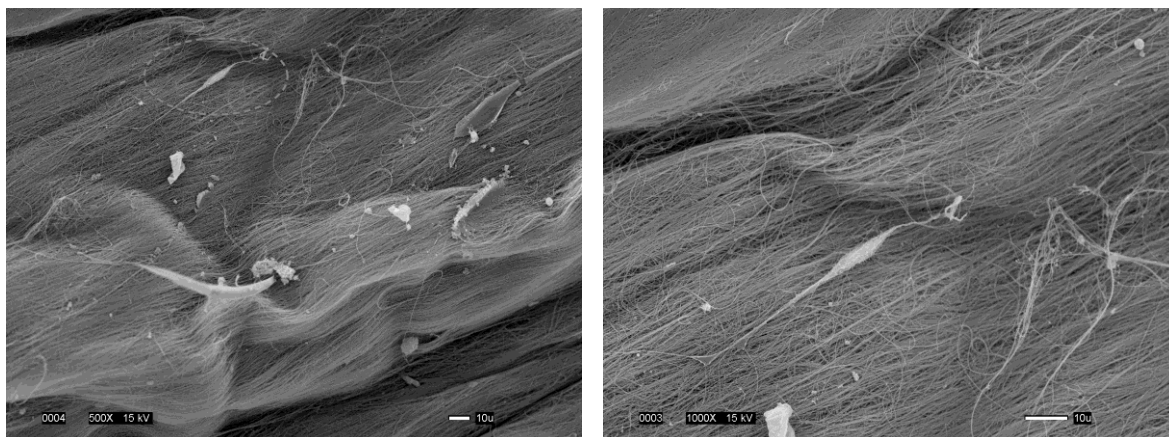


Figure 4.13 (c) Cells attached to the CNT web of the 200 CNT sample

Figure 4.13 (d) Single cell attachment to the CNT web on the 200 CNT sample.

Scale bar: 10 μm .

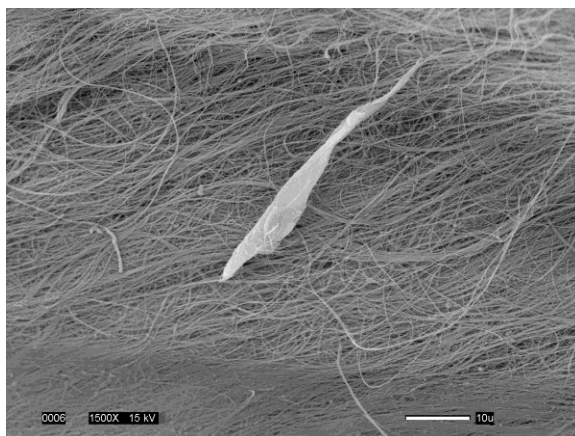


Figure 4.13 (e) Single cell attachment to the CNT web of the 200 CNT sample.

Scale bar: 10 μm .

The above images demonstrate that 3T3 cells can attach to CNT webs. However, the direction of cells growth was not in the direction of the aligned CNTs. This may be explained by the fact that cells could not distinguish their direction. In the future, in order to stimulate the cells to orientate in the direction of aligned CNTs, it may be necessary to apply an electrical potential across the guides during in vitro cell culture. Although the 3T3 fibroblast cells proliferate and attach to the PLA and CNT surfaces in the nerve guides, different cell are likely to behave differently. Schwann cells should be seeded on the prototype nerve guides in the future to identify whether these nerve conduits with CNTs can improve the attachment and migration of Schwann cells. Figure 4.14 shows the attachment of 3T3 cells to the inner PLA tube.

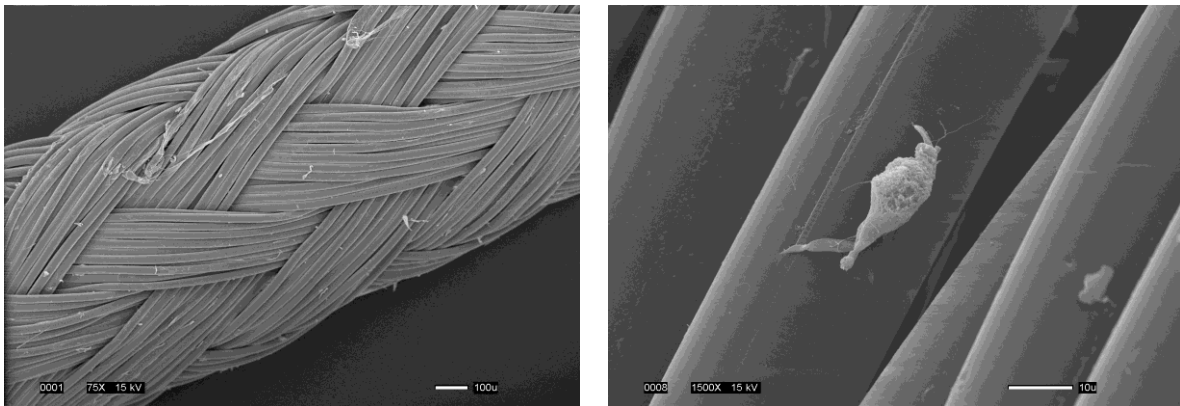


Figure 4.14 (a) 3T3 cells on the inner PLA tube. Scale bar: 100 μ m.

Figure 4.14 (b) A single 3T3 cell attached and aligned on the PLA fibers.

Scale bar: 10 μ m.

CHAPTER 5

CONCLUSIONS AND FUTURE WORK

5.1 Conclusions

A multiple layer nerve guide incorporating carbon nanotubes has been designed and fabricated as described in Chapter 1. The results of the mechanical and biological testing have been presented, discussed and analyzed in Chapter 4. Based on these results, the hypotheses proposed in Chapter 1 can be answered as follows.

1. The braided structure successfully protected the carbon nanotubes, and avoided the possibility of shrinkage during the heat setting treatment. This thermal treatment caused the poly(ethylene oxide) to melt and ensure that the carbon nanotubes to maintain their stability in the liquid culture environment during biological testing.
2. The nerve guides with carbon nanotubes showed improved tensile strength and compression resistance compared to the controls, which indicates that the carbon nanotubes enhanced the stability of the structure. However, there was no significant difference in tensile strength and compression resistance between the samples with

different amounts of carbon nanotubes. This suggests that the concentration of carbon nanotubes had little influence on the mechanical properties of the nerve guide. The lower kinking resistance for the nerve guide sample with carbon nanotubes compared to the controls illustrates that the incorporation of carbon nanotubes reduced the flexibility of the nerve guide.

3. The process of introducing and removing poly(ethylene oxide) reduced the tensile strength but improved cell proliferation, which indicates that the performance of the nerve guides with carbon nanotubes was influenced to some degree by the presence of the poly (ethylene oxide). If no poly(ethylene oxide) had been incorporated within the tubular structure, the tensile strength of the nerve guides with carbon nanotubes might have been even higher.
4. The extent of cell proliferation and attachment within the nerve guides with carbon nanotubes showed similar results to the control samples, which confirms that the biocompatibility of the nerve guides was equivalent regardless of whether the carbon nanotubes were or were not present.
5. The cells did not migrate preferentially in the direction of the carbon nanotubes. This suggests that the aligned carbon nanotubes could not help improve the rate of cell migration in any specific direction without electrical stimulation.

Based on these answers to the specific hypotheses, the main conclusion of the study is that the novel multiple layer nerve guide incorporating aligned carbon nanotubes with a

high surface area was found to be biocompatible and provided superior tensile strength and compression resistance. Therefore, carbon nanotubes have the potential to be an attractive biomaterial is the design of nerve guides for peripheral nerve regeneration.

5.2 Future Work

After evaluation and analysis of this study, and based on the literatures, the following five changes are proposed for future work to achieve improvement of nerve guide with carbon nanotubes and reach the ultimate goal of this study.

1. From the point of view of fabrication, it is proposed that the carbon nanotube web can be fabricated as an inner tube or core. The PLA tubes should then be braided around the core with 36 picks/inch followed by a second braided tube with 48 picks/inch PLA tube to improve the nutrient and oxygen exchange through the pores of the tubular layers during biological testing. In addition, the distance between the carbon nanotube web and the internal PLA tube could be increased so that the cells have more space to grow and migrate.
2. From a materials point of view, poly(ethylene oxide) in the electrospun carbon nanotubes/polymer web layer could be replaced by poly(lactic acid), which is the same resorbable polymer as used in the braided layers. This would remove influence of poly(ethylene oxide).

3. With the intention of increasing the rate and extent of cell migration, electrical stimulation should be applied during the period of cell culture so that the cells experience the electrical stimulation and migrate along the direction of the carbon nanotubes. In addition, altering the level of conductivity is a way to improve the rate of cell migration. For example, a nerve guide could be fabricated with a high conductivity section followed by a low conductivity section, which could then be continuous to another high conductivity section along its length. It is possible that such a “conductivity gradient” would work like a growth factor.
4. With the focus on nerve regeneration, the cells used for the biological culture test should be changed to Schwann cells. This may lead to the formation of “bands of Bünger” which would confirm that nerve guides with carbon nanotubes could improve peripheral nerve regeneration.
5. In order to undertake further evaluation for clinical applications, it will be necessary to undertake an animal in vivo study. During this evaluation, the regeneration of axons, the inflammatory response to the injury and the implanted nerve guides, the muscle reaction under nerve stimulation and the movement of the repaired limbs need to be monitored and reported.

REFERENCES

Aldinucci, A., Turco, A., & etc. (2013). Carbon nanotube scaffolds instruct human dendritic cells: Modulating immune responses by contacts at the nanoscale. - *Nano Lett.* 2013 Dec 11;13(12):6098-105.

Antonio Merolli, Thomas J. Joyce, eds., Frédéric Schuind., & Merolli, A. (. (2009). *Biomaterials in hand surgery*. Dordrecht ; New York: Springer.

Arslantunali, D., Budak, G., & Hasirci, V. (2014). Multiwalled CNT-pHEMA composite conduit for peripheral nerve repair. *Journal of Biomedical Materials Research Part A*, 102(3), 828-841.

Astete, C. E., & Sabliov, C. M. (2006). Synthesis and characterization of PLGA nanoparticles. *Journal of Biomaterials Science -- Polymer Edition*, 17(3), 247-289.

ASTM International. (2001). *ASTM D6571-01 standard test method for determination of compression resistance and recovery properties of highloft nonwoven fabric using static force loading*. ASTM International.

Bennet, D., & Kim, S. (2011). Implantable microdevice for peripheral nerve regeneration: Materials and fabrications. *Journal of Materials Science*, 46(14), 4723-4740.

Birch, R. (2013). *Peripheral nerve injuries: A clinical guide*. London: Springer.

Brenner, M. J., Lowe, J. B., & Fox, I. K. (2005). Effects of schwann cells and donor antigen on long-nerve allograft regeneration. *Microsurgery*, 25(1), 61-70.

Briassoulis, D. (2004). An overview on the mechanical behaviour of biodegradable agricultural films. *Journal of Polymers and the Environment*, 12(2), 65-81. √

Carbrey, J. (2014). *Introductory human physiology*. Unpublished manuscript.

Cellot, G., Toma, F., & etc. (2011). Carbon nanotube scaffolds tune synaptic strength in cultured neural circuits: Novel frontiers in nanomaterial-tissue interactions. - *J Neurosci*. 2011 Sep 7;31(36):12945-53.

Chandra, R., & Rustgi, R. (1998). Biodegradable polymers. *Progress in Polymer Science*, 23(7), 1273-1335.

Cheap Tubes Inc. (2014). Multi walled carbon naotubes-MWNTs. Retrieved Retrieved from <http://www.cheaptubes.com/mwnts.htm>

Chen, C., Soni, S., Le, C., Biasca, M., Farr, E., Chen, E. -, & Chin, W. (2012). Human stem cell neuronal differentiation on silk-carbon nanotube composite. *Nanoscale Research Letters*, 7(1), 1-7.

Ebbesen, T. W., Lezec, H. J., Hiura, H., & Bennett, J. W. (1996). Electrical conductivity of individual carbon nanotubes. *Nature*, 382(6586), 54-56.

Emanuel, N., Neuman, M., & Barak, S. In Polypid Ltd. (Ed.), *Sustained-release drug carrier*

Evans, G. R. D. (2001). Peripheral nerve injury: A review and approach to tissue engineered constructs. *The Anatomical Record*, 263(4), 396-404.

Fabbro A, Sucapane A, & etc. (2013). Adhesion to carbon nanotube conductive scaffolds forces action-potential appearance in immature rat spinal neurons. - *PLoS One*, 8(8)

Fratzl, P. (2008). In edited by Peter Fratzl., Fratzl P. (Eds.), *Collagen : Structure and mechanics*. New York: Springer.

Galvan-Garcia, P., Keefer, E. W., & Yang, F. (2007). Robust cell migration and neuronal growth on pristine carbon nanotube sheets and yarns. *Journal of Biomaterials Science -- Polymer Edition*, 18(10), 1245-1261.

General Cable. (2014). Cable design equations - braid shield. Retrieved Retrieved from http://www.digikey.com/Web%20Export/Supplier%20Content/GenCable_42/PDF/GC_CableDesignEquationsBraidShield.pdf?redirected=1

Gevorkian, S. G., Allahverdyan, A. E., Gevorgyan, D. S., Simonian, A. L., & Hu, C. (2013). Stabilization and anomalous hydration of collagen fibril under heating. *Plos One*, 8(11), 1-11.

Gordon, T., Sulaiman, O., & Boyd, J. G. (2003). Experimental strategies to promote functional recovery after peripheral nerve injuries. *Journal of the Peripheral Nervous System*, 8(4), 236-250.

Griffin, J. W., Hogan, M. V., Chhabra, A. B., & Deal, D. N. (2013). Peripheral nerve repair and reconstruction. *The Journal of Bone & Joint Surgery*, 95(23), 2144-2151. Retrieved from <http://dx.doi.org/10.2106/JBJS.L.00704>.

Hedhli, L. (2011). *Polymerization of fluoropolymers using polycaprolactone* Google Patents. Retrieved from <http://www.google.com/patents/EP2274345A2?cl=en>.

Huang, Y., & Hsu, S. (2011). Effects of laminin-coated carbon nanotube/chitosan fibers on guided neurite growth. - *J Biomed Mater Res A*.2011 Oct; 99(1):86-93.

Huang, Y., Wu, H., Tai, N., & Wang, T. (2012). Carbon nanotube rope with electrical stimulation promotes the differentiation and maturity of neural stem cells. *Small*, 8(18), 2869-2877.

Integra LifeScience Corporation. (2010). NeuraGen nerve guide. Retrieved Retrieved from <http://www.ilstraining.com/NTC%20Solutions/brochures.html>.

Jang, M., & Namgung, S. (2010). Directional neurite growth using carbon nanotube patterned substrates as a biomimetic cue. *Nanotechnology*.2010 Jun 11; 21(23):235102.

Jin GZ, Kim M. (2011). Effect of carbon nanotube coating of aligned nanofibrous polymer scaffolds on the neurite outgrowth of PC-12 cells. - *Cell Biol Int.* 2011 Jul; 35(7):741-5.

Kehoe, S., Zhang, X. F., & Boyd, D. (2012). FDA approved guidance conduits and wraps for peripheral nerve injury: A review of materials and efficacy. *Injury*, 43(5), 553-572.

Kim, Y., & Kim, J. Differential stimulation of neurotrophin release by the biocompatible nano-material (carbon nanotube) in primary cultured neurons. - *J Biomater Appl.* 2014 Jan; 28(5):790-7

Lee, B., Ju, Y. M., Cho, J., Jackson, J. D., Lee, S. J., Atala, A., & Yoo, J. J. (2012). End-to-side neurorrhaphy using an electrospun PCL/collagen nerve conduit for complex peripheral motor nerve regeneration. *Biomaterials*, 33(35), 9027-9036.

Lee, W., & Parpura, V. Chapter 6 - carbon nanotubes as substrates/scaffolds for neural cell growth. *Progress in brain research* (pp. 110-125) Elsevier.

Li, R., Liu, Z., Pan, Y., Chen, L., Zhang, Z., & Lu, L. (2014). Peripheral nerve injuries treatment: A systematic review. *Cell Biochemistry and Biophysics*, 68(3), 449-454.

Liang, J. (2013). *A braided double layer nerve conduit for peripheral nerve regeneration*. (Unpublished Master of Science). North Carolina State University, Textile Engineering.

Liang, D., Hsiao, B. S., & Chu, B. (2007). Functional electrospun nanofibrous scaffolds for biomedical applications. *Advanced Drug Delivery Reviews*, 59(14), 1392-1412.

lifetechnologies. (2014). MTT assay protocol. Retrieved Retrieved from <http://www.lifetechnologies.com/us/en/home/references/protocols/cell-culture/mtt-assay-protocol/vybrant-mtt-cell-proliferation-assay-kit.html>

Liu, Y., Zhao, Y., Sun, B., & Chen, C. Understanding the toxicity of carbon nanotubes. *Accounts of Chemical Research*, (3), 702.

M Meyyappan and Lance Delzeit and Alan Cassell and, David Hash. (2003). Carbon nanotube growth by PECVD: A review. *Plasma Sources Science and Technology*, 12(2), 205. Retrieved from <http://stacks.iop.org/0963-0252/12/i=2/a=312>

Mackinnon, S. E., & Dellon, A. L. (January, 1988). *Surgery of peripheral nerve* (1st ed.) Thieme Publishing Group.

Mackinnon, S. E., & Dellon, A. L. (March 1990). Clinical nerve construction with a bioabsorbable polyglycolic acid tube. *Plastic & Reconstructive Surgery*, 85(3), 419-424.

Maharana, T., Mohanty, B., & Negi, Y. S. (2009). Melt–solid polycondensation of lactic acid and its biodegradability. *Progress in Polymer Science*, 34(1), 99-124.

Marquardt, L. M., & Sakiyama-Elbert, S. (2013). Engineering peripheral nerve repair. *Current Opinion in Biotechnology; Tissue, Cell and Engineering*, 24(5), 887-892.

Matejka, V. (2002). Peripheral nerve reconstruction by autograft. *Injury*, 33(7), 627-631.

Matteo Santin, e., & Santin, M. (2009), *Strategies in regenerative medicine: Integrating biology with materials design*. New York; London: Springer.

Merolli, A., & Rocchi, L. (2009). Peripheral nerve regeneration by artificial nerve guides. In A. Merolli, & T. Joyce (Eds.), (pp. 127-143) Springer Milan.

Mishra, A. K. (2012). *Nanotechnology science and technology: Carbon nanotubes: Synthesis and properties*. New York, NY, USA: Nova Science Publishers, Inc.

Mottaghitab F, Farokhi M, & etc. (2013). A biosynthetic nerve guide conduit based on silk/SWNT/fibronectin nanocomposite for peripheral nerve regeneration. - *PLoS One*, 8(9), 74417.

Niyogi, S., Hamon, M. A., Hu, H. (2002). Chemistry of single-walled carbon nanotubes. *Accounts of Chemical Research*, 35(12), 1105-1113.

Perego, G., Cella, G. D., & Bastioli, C. (1996). Effect of molecular weight and crystallinity on poly(lactic acid) mechanical properties. *Journal of Applied Polymer Science*, 59(1), 37-43.

Polyganics. (2014). vivosorb/polyganics. Retrieved Retrieved from <http://www.polyganics.com/solutions/peripheral-nerve-repair/vivosorb>

Poore, T. (2007). Multi-walled carbon naotube. Retrieved from <http://archimorph.com/2007/09/07/3ds-max-drawing-and-rendering-of-a-multi-wall-nanotube/>

Schmid, E. (2012). Chapter 10 central nervous system, spinal and cranial nerves. Retrieved from <http://classroom.sdmesa.edu/eschmid/Chapter10-Zoo145.htm> Quigley, A. F., Bulluss, K. J., etc. (2013). Engineering a multimodal nerve conduit for repair of injured peripheral nerve. *Journal of Neural Engineering*, 10(1), 016008. Retrieved from <http://stacks.iop.org/1741-2552/10/i=1/a=016008>

Ratner, B. D., Hoffman, A. S., & Schoen, F. J. (2012). *Biomaterials science : An introduction to materials in medicine (3rd edition)*. Saint Louis, MO, USA: Academic Press.

Ray, W. Z., & Mackinnon, S. E. (2010). Management of nerve gaps: Autografts, allografts, nerve transfers, and end-to-side neurorrhaphy. *Experimental Neurology; Regeneration in the Peripheral Nervous System*, 223(1), 77-85.

Reid, A. J., de Luca, A. C., Faroni, A., Downes, S., Sun, M., Terenghi, G., & Kingham, P. J. (2013). Long term peripheral nerve regeneration using a novel PCL nerve conduit. *Neuroscience Letters*, 544(0), 125-130.

Rutkowski, G. E., & Heath, C. A. (2002). Development of a bioartificial nerve graft. II. nerve regeneration in vitro. *Biotechnology Progress*, 18(2), 373-3

Serrano, M. C., Gutiérrez, M. C., & del Monte, F. Role of polymers in the design of 3D carbon nanotube-based scaffolds for biomedical applications. *Progress in Polymer Science*. In press.

Södergård, A., & Stolt, M. (2002). Properties of lactic acid based polymers and their correlation with composition. *Progress in Polymer Science*, 27(6), 1123-1163.

Son, W. K., Youk, J. H., Lee, T. S., & Park, W. H. (2004). The effects of solution properties and polyelectrolyte on electrospinning of ultrafine poly(ethylene oxide) fibers. *Polymer*, 45(9), 2959-2966.

Sulaiman, W., & Gordon, T. (2013). Neurobiology of peripheral nerve injury, regeneration, and functional recovery: From bench top research to bedside application. *The Ochsner Journal*, 13(1), 100-100.

Sun, M., Kingham, P. J., Reid, A. J., Armstrong, S. J. (2010). In vitro and in vivo testing of novel ultrathin PCL and PCL/PLA blend films as peripheral nerve conduit. *Journal of Biomedical Materials Research. Part A*, 93(4), 1470-1481.

Syed, N. I. (2009). Peripheral nerve injury, repair, and regeneration. (pp. 321-340). New York, NY: Springer New York.

Vroman, I., & Tighzert, L. (2009). Biodegradable polymers. *Materials*, 2(2), 307-344.

Retrieved from <http://www.mdpi.com/1996-1944/2/2/307>

Xie, F., Li, Q. F., Gu, B., Liu, K., & Shen, G. X. (2008). In vitro and in vivo evaluation of a biodegradable chitosan-PLA composite peripheral nerve guide conduit material. *Microsurgery*, 28(6), 471-479.

Yu, W., Zhang, Z., Jiang, X.. (2014). A novel electrospun nerve conduit enhanced by carbon nanotubes for peripheral nerve regeneration. *Nanotechnology*, 25(16), 165102.

Zhao, W., Yu, W., Zheng, J., Wang, Y., Zhang, Z., & Zhang, D. (2014). Effects of carbon nanotubes in a Chitosan/Collagen-based composite on mouse fibroblast cell proliferation. *Cellular and Molecular Neurobiology*, 34(1), 43-50

Zochodne, D. W. (2008). *Neurobiology of peripheral nerve regeneration*. Cambridge, UK; New York: Cambridge University Press.